Tropomodulin isoforms regulate thin filament pointed-end capping and skeletal muscle physiology

David S. Gokhin,[1,2,3] Raymond A. Lewis,[1] Caroline R. McKeown,[1] Roberta B. Nowak,[1] Nancy E. Kim,[1] Ryan S. Littlefield,[4] Richard L. Lieber,[2,3] and Velia M. Fowler[1]

[1]Department of Cell Biology, The Scripps Research Institute, La Jolla, CA 92037
[2]Department of Bioengineering and [3]Department of Orthopaedic Surgery, University of California, San Diego, La Jolla, CA 92093
[4]Center for Cell Dynamics, Friday Harbor Laboratories, University of Washington, Friday Harbor, WA 98250

During myofibril assembly, thin filament lengths are precisely specified to optimize skeletal muscle function. Tropomodulins (Tmods) are capping proteins that specify thin filament lengths by controlling actin dynamics at pointed ends. In this study, we use a genetic targeting approach to explore the effects of deleting Tmod1 from skeletal muscle. Myofibril assembly, skeletal muscle structure, and thin filament lengths are normal in the absence of Tmod1. Tmod4 localizes to thin filament pointed ends in Tmod1-null embryonic muscle, whereas both Tmod3 and -4 localize to pointed ends in Tmod1-null adult muscle. Substitution by Tmod3 and -4 occurs despite their weaker interactions with striated muscle tropomyosins. However, the absence of Tmod1 results in depressed isometric stress production during muscle contraction, systemic locomotor deficits, and a shift to a faster fiber type distribution. Thus, Tmod3 and -4 compensate for the absence of Tmod1 structurally but not functionally. We conclude that Tmod1 is a novel regulator of skeletal muscle physiology.

Introduction

The precise regulation of actin filament assembly is critical for cytoskeletal architecture in many cellular processes, including migration, shape maintenance, and contractile function. A striking example of strictly orchestrated actin filament assembly is found in skeletal muscle cells, where semicrystalline arrays of actin (thin) and myosin (thick) filaments comprise the contractile apparatus (Clark et al., 2002). In sarcomeres, thin filament fast-growing (barbed) ends are anchored in the Z-line, and their slow-growing (pointed) ends extend into the middle of the sarcomere, terminating at the H-zone. Thin filaments are extremely uniform in length but dynamic at their ends, where new actin monomer can be incorporated by subunit exchange (Littlefield et al., 2001). Thin filament pointed ends are capped by tropomodulins (Tmods), which interact with tropomyosins (TMs) and cap TM-decorated actin ends more tightly than bare actin ends (Weber et al., 1994, 1999; Kostyukova et al., 2005, 2006). Tmod-mediated pointed-end dynamics are a key regulator of thin filament length in mammalian cardiac muscle and invertebrate striated muscles (for review see Littlefield and Fowler, 2008), but Tmod's roles in thin filament length regulation in skeletal muscle and how thin filament length regulation influences in vivo skeletal muscle physiology remain unknown.

Tmods may regulate thin filament length in skeletal muscle through several mechanisms. Mammalian skeletal muscle contains nebulin, a giant rodlike protein that coextends with actin along thin filaments (McElhinny et al., 2003). Nebulin has been proposed to be a molecular ruler that determines the position of Tmod relative to the Z-line, thereby specifying thin filament length (Kruger et al., 1991; Labeit et al., 1991; McElhinny et al., 2001; for review see Littlefield and Fowler, 2008). However, recent evidence challenges this model because nebulin does not coextend with actin along the entire thin filament (Castillo et al., 2009). Rather, a nebulin-free actin pointed-end extension demarcates the periphery of the H-zone (Castillo et al., 2009). The lengths of the actin filament extensions past the N terminus of nebulin vary across skeletal muscles, determining muscle-specific thin filament lengths and sarcomere length–tension

D.S. Gokhin and R.A. Lewis contributed equally to this paper.

Correspondence to Velia M. Fowler: velia@scripps.edu

Abbreviations used in this paper: EDL, extensor digitorum longus; MHC, myosin heavy chain; PCSA, physiological cross-sectional area; TA, tibialis anterior; TEM, transmission EM; TM, tropomyosin; Tmod, tropomodulin.

The Rockefeller University Press $30.00
J. Cell Biol. Vol. 189 No. 1 95–109
www.jcb.org/cgi/doi/10.1083/jcb.201001125

relationships (Granzier et al., 1991; Castillo et al., 2009). Furthermore, skeletal muscles from nebulin-null mice have shorter and somewhat more variable lengths instead of completely dysregulated lengths that would be expected if nebulin were a true ruler (Bang et al., 2006; Witt et al., 2006). Thus, it has been suggested instead that nebulin stabilizes a large core region of the thin filament, whereas pointed-end actin dynamics (as regulated by Tmods and interactions with TMs) fine-tune uniform filament lengths in skeletal muscle (for review see Littlefield and Fowler, 2008).

Four Tmod isoforms are present within mammals that could allow them to fine-tune thin filament lengths at the pointed end. Tmod1 is expressed predominantly in terminally differentiated, postmitotic cells (such as erythrocytes, lens fiber cells, neurons, and striated muscle), Tmod2 is expressed exclusively in neuronal tissues, Tmod3 is expressed ubiquitously, and Tmod4 is restricted to skeletal muscle in mammals (Fowler, 1987, 1990; Sung et al., 1992; Watakabe et al., 1996; Almenar-Queralt et al., 1999b; Cox and Zoghbi, 2000; Conley et al., 2001). With these expression patterns, Tmod1, -3, and -4 are all potential regulators of pointed-end actin dynamics and thin filament lengths in skeletal muscle sarcomeres. Based on studies in cardiac muscle, changes in overall levels of Tmods via relative isoform expression could affect the extent of pointed-end capping, thus regulating thin filament lengths (for review see Littlefield and Fowler, 2008). Furthermore, at least Tmod1 and -4 have differential binding to TMs (Greenfield and Fowler, 2002; Kostyukova et al., 2006, 2007). Therefore, we hypothesized that a combination of Tmod isoform expression and avidity for TMs regulates thin filament length in skeletal muscles.

To decipher the role of Tmods in regulating thin filament length in skeletal muscle, we used a genetic targeting approach to delete Tmod1 from skeletal muscle. As shown in previous studies using Tmod1-null mice, global deletion of Tmod1 results in failure of cardiac myofibril assembly, contraction, and looping morphogenesis, resulting in embryonic lethality at embryonic day (E) 9.5 (Chu et al., 2003; Fritz-Six et al., 2003). Because this occurs before the onset of skeletal myogenesis, it is impossible to use Tmod1-null mice to determine the role of Tmod1 in skeletal muscle. To surmount this obstacle, our laboratory rescued the lethality of Tmod1-null mice through the use of a cardiac-specific transgene, generating mice that express Tmod1 in the heart but lack Tmod1 in all other tissues, including skeletal muscle (McKeown et al., 2008). In this study, we report that, in contrast to cardiac muscle, Tmod1 is dispensable for the correct specification of thin filament lengths in both embryonic and adult skeletal muscle because Tmod3 and/or -4 is recruited to the pointed ends when Tmod1 is absent. This compensatory regulation of lengths occurs despite the fact that Tmod3 and -4 levels do not change when Tmod1 is absent, and Tmod3 and -4 both interact with striated muscle TMs more weakly than does Tmod1. Surprisingly, we discovered that deletion of Tmod1 depresses skeletal muscle contractile function in a thin filament length–independent manner and shifts fiber types toward a faster composition. This is the first study to provide an in vivo demonstration that particular Tmod isoforms can substitute for one another to maintain correct muscle-specific thin filament lengths in skeletal muscles. However, Tmod isoforms do not substitute for one another functionally, revealing novel functions of Tmods as regulators of skeletal muscle physiology.

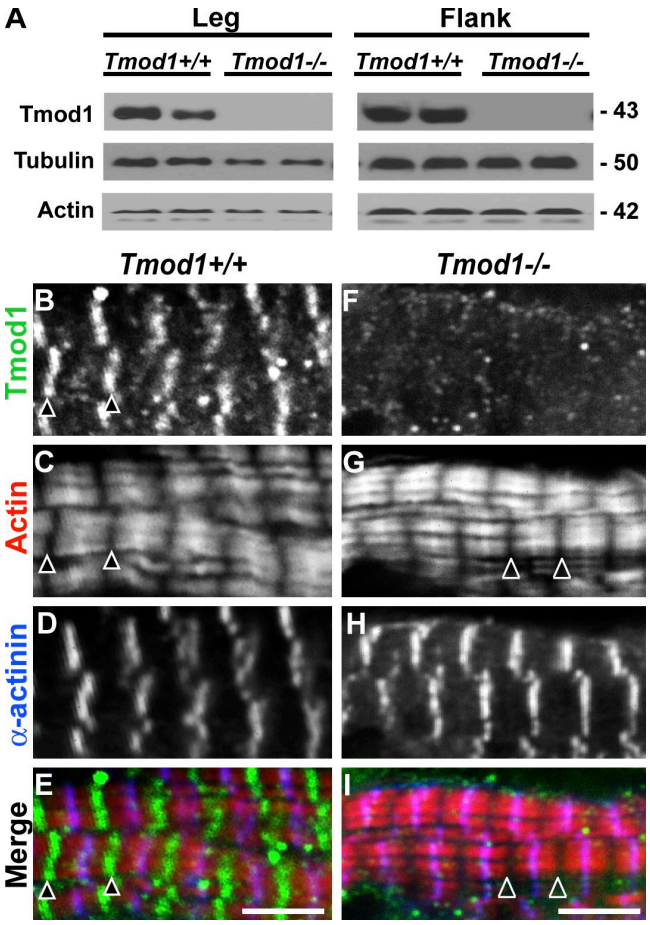

Figure 1. **Tmod1 is dispensable for myofibril assembly.** (A) Western blots of E15.5 mouse embryonic leg and flank muscle tissue lysates show absence of Tmod1 in $Tmod1^{-/-Tg+}$ muscles. Tubulin and actin were loading controls. Molecular mass is indicated in kilodaltons. (B–I) Skeletal muscle from $Tmod1^{+/+}$ and $Tmod1^{-/-Tg+}$ E15.5 mouse embryos stained for Tmod1, F-actin, and α-actinin. Arrowheads denote H-zones. Bars, 3 µm.

Results

Tmod1 is dispensable for skeletal muscle development, myofibrillogenesis, and thin filament length specification

We previously rescued the early embryonic lethality of the Tmod1-null mouse with a cardiac-specific transgene that places Tmod1 under the control of the α myosin heavy chain (α-MHC) promoter ($Tmod1^{-/-Tg(\alpha\text{-}MHC\text{–}Tmod1)}$; hereafter referred to as $Tmod1^{-/-Tg+}$; McKeown et al., 2008). This enabled us to study the requirement of Tmod1 in skeletal myofibril assembly during development, which occurs starting around E13 of mouse embryogenesis (Miller, 1991). As expected from the absence of Tmod1 expression in the noncardiac tissues of $Tmod1^{-/-Tg+}$ mice (McKeown et al., 2008; Nowak et al., 2009), Western blotting of E15.5 embryonic leg and flank skeletal muscle lysates demonstrated the absence of Tmod1 from $Tmod1^{-/-Tg+}$ embryos (Fig. 1 A). Tmod1 staining was

Table I. **Thin filament length parameters determined by distributed deconvolution analysis of fluorescence images**

Muscle type	Phalloidin			Nebulin M1M2M3			Tmod		
	Mean ± SD	Min–max	*n*	Mean ± SD	Min–max	*n*	Mean ± SD	Min–max	*n*
	μm	*μm*		*μm*	*μm*		*μm*	*μm*	
Embryonic flank									
Tmod1$^{+/+}$	1.18 ± 0.09	1.02–1.35	122	0.86 ± 0.04	0.77–0.98	57	1.23 ± 0.10	1.09–1.50	27
Tmod1$^{-/-Tg+}$	1.19 ± 0.06	1.07–1.36	100	0.85 ± 0.04	0.75–0.97	94	1.26 ± 0.07	1.13–1.40	43
Adult EDL									
Tmod1$^{+/+}$	1.06 ± 0.07	0.92–1.25	79	0.84 ± 0.07	0.68–1.06	50	1.11 ± 0.06	0.92–1.27	67
Tmod1$^{-/-Tg+}$	1.07 ± 0.06	0.94–1.21	67	0.85 ± 0.04	0.75–1.00	61	1.13 ± 0.09	0.89–1.33	82
Adult soleus									
Tmod1$^{+/+}$	1.15 ± 0.07	0.95–1.29	86	0.90 ± 0.05	0.83–1.03	50	1.22 ± 0.08	1.02–1.34	42
Tmod1$^{-/-Tg+}$	1.16 ± 0.07	1.00–1.31	114	0.89 ± 0.03	0.81–0.96	52	1.22 ± 0.06	1.11–1.37	51

Min, minimum; max, maximum. All lengths are in micrometers from the Z-line, measured from *n* myofibrils from three to four mice per genotype. All nebulin M1M2M3 lengths were significantly closer to the Z-line than corresponding Tmod lengths ($P < 10^{-38}$). For embryonic flank phalloidin, nebulin M1M2M3, and Tmod, P = 0.08, P = 0.64, and P = 0.14, respectively. For adult EDL phalloidin, nebulin M1M2M3, and Tmod, P = 0.36, P = 0.48, and P = 0.20, respectively. For adult soleus phalloidin, nebulin M1M2M3, and Tmod, P = 0.39, P = 0.16, and P = 0.87, respectively.

also not detected in cryosections of the embryonic *Tmod1*$^{-/-Tg+}$ skeletal muscle, confirming that the α-MHC promoter is cardiac specific and not leaky (Fig. 1 and Fig. S1; Rindt et al., 1995; Sussman et al., 1998b). Muscle development and myofibril assembly appeared normal, based on normal myotube sizes, alignment, and morphology in cryosections of embryonic muscles (Fig. S1).

To examine myofibrillogenesis during skeletal muscle development in the absence of Tmod1, we performed immunofluorescence staining for α-actinin at the Z-lines and fluorescent phalloidin staining for F-actin on frozen sections of E15.5 *Tmod1*$^{-/-Tg+}$ embryos. Surprisingly, skeletal muscle from *Tmod1*$^{-/-Tg+}$ embryos was striated and appeared to have regulated thin filament lengths, as demonstrated by uniform gaps in F-actin at the H-zone and regular periodic striations of α-actinin (Fig. 1). Thus, in stark contrast to cardiac muscle (Chu et al., 2003; Fritz-Six et al., 2003), skeletal muscle myofibrillogenesis, including the assembly of thin filaments with regulated lengths, does not require Tmod1. Next, using phalloidin staining for F-actin to visualize thin filaments, we measured thin filament lengths by distributed deconvolution analysis (Littlefield and Fowler, 2002). Surprisingly, we found that *Tmod1*$^{+/+}$ and *Tmod1*$^{-/-Tg+}$ embryonic muscles had statistically indistinguishable thin filament lengths of ∼1.2 μm (Table I), indicating that Tmod1 is not necessary to specify thin filament length in skeletal muscle in vivo. Thus, we conclude that developing skeletal muscle possesses a Tmod1-independent mechanism to specify thin filament length that is not present in cardiac muscle.

The giant protein nebulin is a skeletal muscle–specific binding partner of Tmod1 and has been proposed to act together with Tmods to regulate skeletal muscle thin filament lengths (Kruger et al., 1991; Labeit et al., 1991; McElhinny et al., 2001). Although loss of Tmod1 did not affect myofibril assembly, we reasoned that nebulin localization might be perturbed in *Tmod1*$^{-/-Tg+}$ embryonic muscle. To address this possibility, we stained embryonic skeletal muscle with antibodies generated against the N-terminal M1M2M3 domain of nebulin (Castillo et al., 2009). The nebulin M1M2M3 domain contains the Tmod1-binding site and localizes near the H-zone boundary where the thin filament pointed ends reside (McElhinny et al., 2001). Although *Tmod1*$^{-/-Tg+}$ embryos completely lacked Tmod1 in their skeletal muscle, nebulin still assembled into sarcomeres and coextended along thin filaments, as indicated by normal M1M2M3 staining (Fig. 2). We also measured no changes in the localization of the M1M2M3 domain with respect to the distance from the Z-line, as determined by distributed deconvolution (Table I). Importantly, the thin filament pointed ends continued to extend beyond the nebulin N terminus, with the filament ends ∼1.2 μm from the Z-line and the M1M2M3 domain ∼0.85 μm from the Z-line (Table I), which is qualitatively similar to observations in rabbit muscles

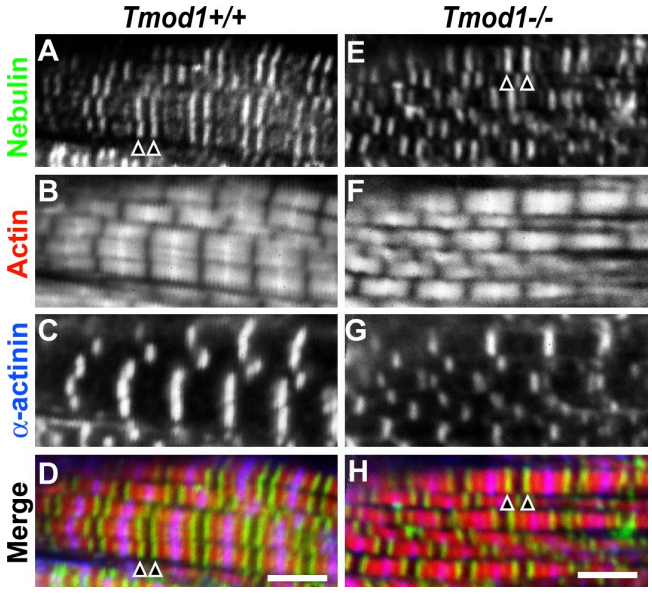

Figure 2. **Tmod1 is dispensable for correct localization of nebulin.** (A–H) Skeletal muscle from *Tmod1*$^{+/+}$ (A–D) and *Tmod1*$^{-/-Tg+}$ (E–H) E15.5 mouse embryos was stained for nebulin M1M2M3, F-actin, and α-actinin. Arrowheads denote nebulin M1M2M3 stripes flanking the H-zone. Bars, 3 μm.

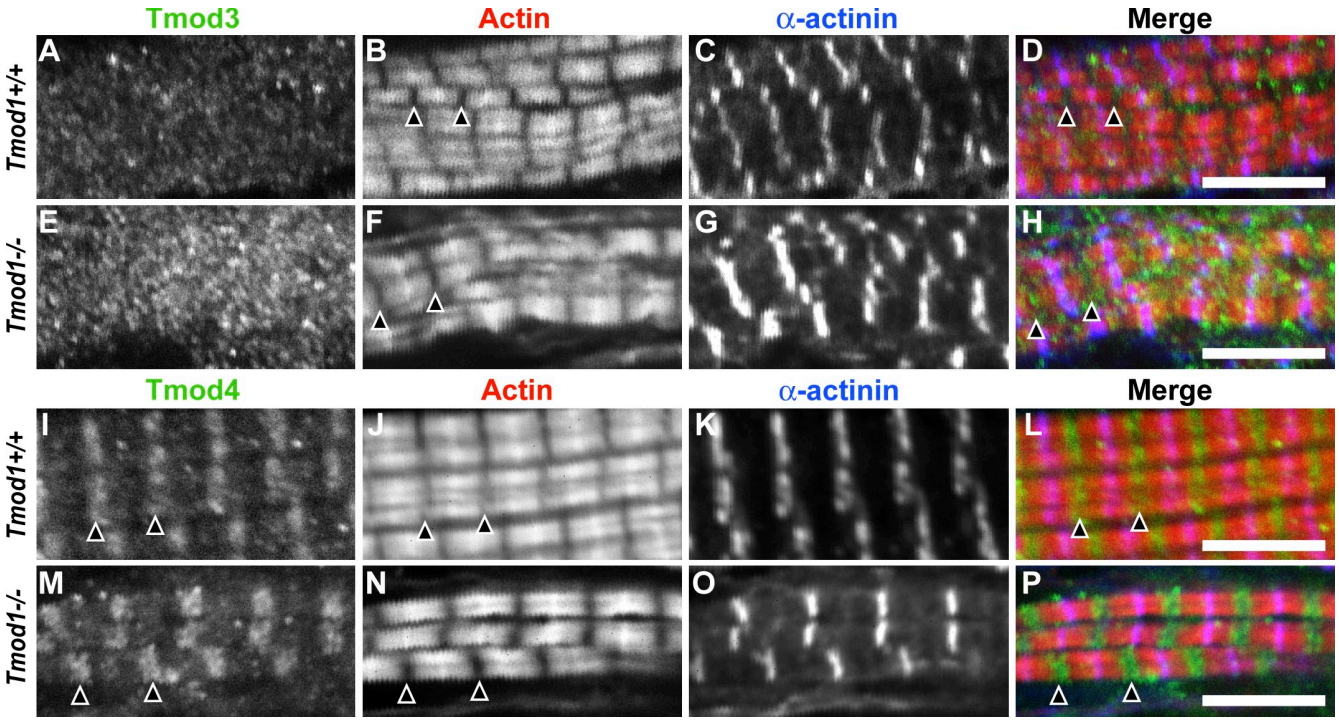

Figure 3. **Tmod4 but not Tmod3 substitutes for Tmod1 by capping thin filament pointed ends in embryonic muscle.** (A–P) Skeletal muscle from *Tmod1*$^{+/+}$ (A–D and I–L) and *Tmod1*$^{-/-Tg+}$ (E–H and M–P) E15.5 mouse embryos stained for F-actin, α-actinin, and either Tmod3 or -4. Tmod3 is diffusely localized, whereas Tmod4 localizes to the pointed ends in the presence or absence of Tmod1. Arrowheads denote H-zones. Bars, 5 µm.

(Castillo et al., 2009). Thus, nebulin is properly localized even in the absence of Tmod1.

Tmod4 but not Tmod3 substitutes for Tmod1 in embryonic skeletal muscle

In the absence of Tmod1, embryonic skeletal muscle thin filaments still have the correct length. We reasoned that Tmod3 and -4 isoforms, which are also expressed in striated muscles, could be substituting for Tmod1 and capping thin filament pointed ends in *Tmod1*$^{-/-Tg+}$ skeletal muscle. Immunofluorescence staining of cryosectioned embryos shows that the distribution of Tmod3, the ubiquitous Tmod isoform, appeared to be diffuse and was not localized to pointed ends in either *Tmod1*$^{+/+}$ or *Tmod1*$^{-/-Tg+}$ embryonic skeletal muscle (Fig. 3, A–H). In contrast, Tmod4, the skeletal muscle–specific isoform, localized at thin filament pointed ends in embryonic skeletal muscle of both *Tmod1*$^{+/+}$ and *Tmod1*$^{-/-Tg+}$ mice (Fig. 3, I–P). Although staining for Tmod4 at the pointed ends in *Tmod1*$^{+/+}$ muscle could potentially be caused by some antibody cross-reactivity with Tmod1, this cannot account for pointed-end staining in *Tmod1*$^{-/-Tg+}$ embryonic muscles in which Tmod1 is not present. Thus, Tmod4 does indeed localize to pointed ends in the absence of Tmod1. Next, we performed distributed deconvolution measurements and found that length measurements based on Tmod localization corroborated those observed with phalloidin staining. Thin filament pointed ends, as measured by Tmod4 localization in *Tmod1*$^{-/-Tg+}$ embryonic muscle and by both Tmod1 and -4 localization in *Tmod1*$^{+/+}$ muscle, were the same distance from the Z-line (Table I). Thus, Tmod4 but not Tmod3 substitutes for Tmod1 in *Tmod1*$^{-/-Tg+}$ embryonic muscle.

Tmod1 is dispensable for the structure of adult skeletal muscle

Tmod1 is not required for embryonic skeletal muscle development (Fig. 1 and Fig. S1), but Tmod1 still could be important for the maintenance of adult muscle structure during contraction and use. Thus, we investigated the properties of skeletal muscle from musculoskeletally mature (1 mo old) *Tmod1*$^{+/+}$ and *Tmod1*$^{-/-Tg+}$ animals (Gokhin et al., 2008). Coomassie-stained gels of skeletal muscle lysates showed no obvious differences in the major protein composition of various muscles, including the tibialis anterior (TA), diaphragm, extensor digitorum longus (EDL), and soleus (Fig. S2), which reflect a variety of fiber type compositions and muscle architectures (Burkholder et al., 1994). Transmission EM (TEM) of the EDL did not reveal any obvious ultrastructural differences between *Tmod1*$^{+/+}$ and *Tmod1*$^{-/-Tg+}$ muscles, with *Tmod1*$^{-/-Tg+}$ muscles exhibiting intact Z- and M-lines, no evidence of split or degenerated myofibrils, and no signs of swollen or aggregated mitochondria (Fig. 4 A). We next used immunofluorescence staining to visualize various constituents of adult myofibrils, including α-actinin (a structural element of the Z-line), the C-terminal M160–164 repeat domain of nebulin (also in the Z-line), and myomesin (a structural element of the M-line). No differences in the sarcomeric localizations of any of these proteins could be found between *Tmod1*$^{+/+}$ and *Tmod1*$^{-/-Tg+}$ muscles (Fig. 4, B–D). Moreover, confocal fluorescence microscopy and low magnification TEM of EDL and soleus muscles (Fig. 4 and not depicted) demonstrated that myofibrils were relatively well aligned in 1-mo-old animals of both genotypes. Although adjacent myofibrils were somewhat

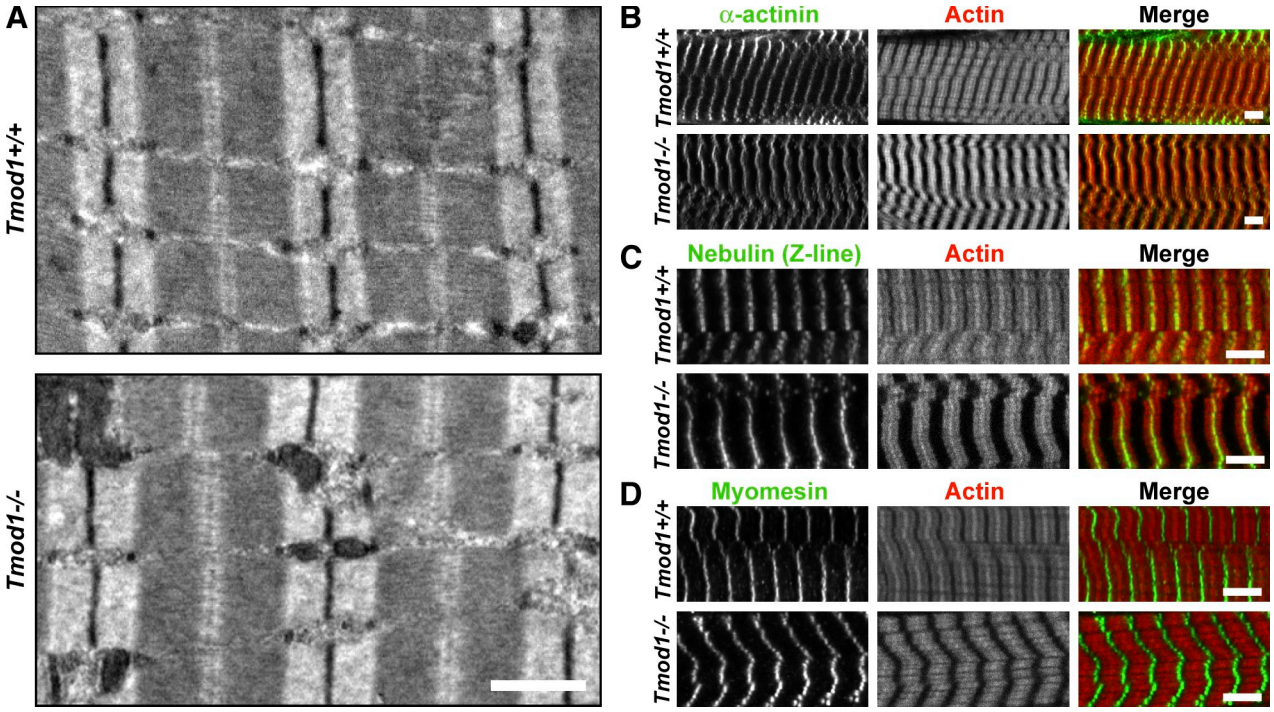

Figure 4. **Tmod1 is dispensable for adult muscle structure.** (A) TEM of 1-mo-old EDL muscle from *Tmod1*$^{+/+}$ and *Tmod1*$^{-/-Tg+}$ mice. (B–D) EDL muscle from *Tmod1*$^{+/+}$ and *Tmod1*$^{-/-Tg+}$ mice stained for F-actin and either α-actinin (B), the C-terminal M160–164 domain of nebulin (C), or myomesin (D). Bars: (A) 1 µm; (B–D) 3 µm.

misaligned in embryonic skeletal muscles of both genotypes, this is characteristic of normal muscle development (Figs. 1–3 and not depicted). These data confirm that *Tmod1*$^{-/-Tg+}$ muscles lack an acute structural pathology.

To test the possibility that Tmod1 might play a role in the maintenance of thin filament length during use of adult muscle, we used distributed deconvolution to measure thin filament lengths (as determined by phalloidin staining for F-actin) and the position of the nebulin M1M2M3 domain in myofibrils from the EDL and soleus muscles of adult *Tmod1*$^{+/+}$ and *Tmod1*$^{-/-Tg+}$ mice. As in embryonic muscles, we found no significant effect of deleting Tmod1 on thin filament length or on the localization of the nebulin M1M2M3 domain in adult skeletal muscle (Table I). Therefore, the Tmod1-independent mechanism that specifies thin filament length in embryonic muscle persists into adulthood and is not compromised by muscle use. Thin filament length in the mouse soleus was ∼0.1 µm longer than in the EDL regardless of the presence of Tmod1, which is consistent with previous studies that have shown that thin filament lengths are muscle specific and longer in slow as compared with fast muscles (Granzier et al., 1991; Bang et al., 2006; Castillo et al., 2009).

Both Tmod3 and -4 substitute for Tmod1 in adult skeletal muscle

We showed that Tmod4 but not Tmod3 could substitute for Tmod1 in embryonic muscle by capping thin filament pointed ends and correctly regulating thin filament length during myofibrillogenesis (Fig. 3 and Table I). Therefore, we reasoned that a similar phenomenon might occur in adult muscle. Western blotting for Tmod1 confirmed that Tmod1 was completely absent from *Tmod1*$^{-/-Tg+}$ adult EDL muscle (Fig. 5 A). However, both Tmod3 and -4 were present in *Tmod1*$^{-/-Tg+}$ EDL muscle at levels that are not qualitatively different from those observed in *Tmod1*$^{+/+}$ muscle (Fig. 5 A). These results were also observed in adult TA, diaphragm, and soleus muscles (Fig. S3). Immunofluorescence staining of EDL muscles revealed that both Tmod3 and -4 have the potential to substitute for Tmod1 in capping thin filaments. As expected, Tmod1 localized to the pointed ends of the thin filaments in *Tmod1*$^{+/+}$ muscle but was undetectable in *Tmod1*$^{-/-Tg+}$ muscle (Fig. 5 B). In contrast, Tmod3 localized weakly to regions on either side of the Z-line as well as to the M-line in *Tmod1*$^{+/+}$ muscle, but when Tmod1 was deleted, Tmod3 redistributed from these regions to the thin filament pointed ends (Fig. 5 C). In contrast, Tmod4 localized to the thin filament pointed ends regardless of the presence of Tmod1 (Fig. 5 D). Therefore, both Tmod3 and -4 can substitute for Tmod1 in adult skeletal muscle. Analogous immunofluorescence staining experiments on the soleus confirmed that these observations are not EDL specific (Fig. S3). We performed distributed deconvolution analysis and found that length measurements based on Tmod localization corroborated those obtained by F-actin staining. Thus, in EDL and soleus muscles from *Tmod1*$^{-/-Tg+}$ mice, the thin filament pointed ends were the same distance from the Z-line as in *Tmod1*$^{+/+}$ muscle, as determined by Tmod localization (Table I). We conclude that, in adult muscle, pointed-end capping by Tmod3 and -4 regulates the muscle-specific uniformity of thin filament lengths in the absence of Tmod1.

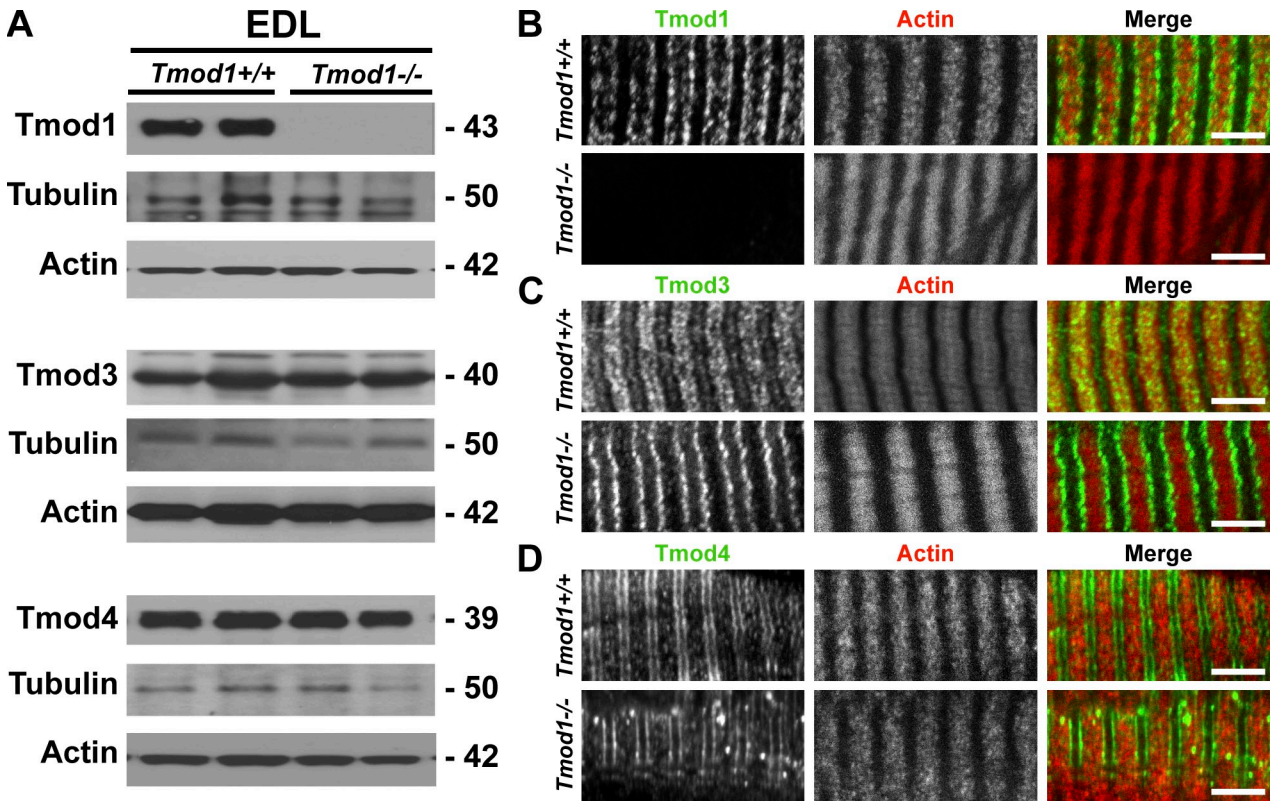

Figure 5. **Tmod3 and -4 substitute for Tmod1 by capping thin filament pointed ends in adult skeletal muscle.** (A) Western blots of 1-mo-old EDL muscle tissue lysates show no apparent changes in Tmod3 or -4 levels in the absence of Tmod1. Tubulin and actin were loading controls. Molecular mass is indicated in kilodaltons. (B–D) EDL muscle from *Tmod1*$^{+/+}$ and *Tmod1*$^{-/-Tg+}$ mice stained for F-actin and either Tmod1 (B), -3 (C), or -4 (D). Bars, 5 µm.

Tmod1 binds to striated muscle TMs more strongly than Tmod3 or -4

We speculated that the absence of Tmod3 at thin filament pointed ends, which are capped by Tmod1 and -4 in *Tmod1*$^{+/+}$ muscle, might be caused by differences in Tmods' avidities for TMs associated with thin filaments. To investigate this possibility, we performed blot overlay experiments to determine the relative binding strengths of Tmod1, -3, and -4 to the striated muscle TMs that are present on sarcomeric thin filaments in embryonic and adult skeletal muscles, α_{slow}-TM and β-TM (Gunning et al., 2008). Tmods bind to the N-terminal end of TMs (Sung and Lin, 1994; Vera et al., 2000; Greenfield and Fowler, 2002), and the N-terminal sequence of α_{fast} striated muscle TM is identical to that of β-TM (Stone and Smillie, 1978; Helfman et al., 1986). In addition, M9R mutant α_{slow}-TM was used as a negative control for Tmod1 binding because it has been shown previously that Tmod1 does not bind to the M9R mutant α_{slow}-TM (Akkari et al., 2002; Ilkovski et al., 2008). To compare relative binding of each TM to the different Tmods, blots containing Tmods were overlaid with the three TMs. The results show that striated muscle TMs recognized Tmod1 better than they recognized Tmod3 or -4; when compared with Tmod1, both α_{slow}-TM and β-TM bound more weakly to Tmod4 and almost not at all to Tmod3 (Fig. 6, A, C, and D). As expected, M9R α_{slow}-TM did not bind to Tmod1 or -4, although it did bind weakly to Tmod3 (Fig. 6, A, C, and D). These data indicate, first, that the absence of capping of thin filament pointed ends by Tmod3 in wild-type muscle can be explained by a lower binding avidity of Tmod3 for striated muscle TMs as compared with Tmod1 and -4. Second, in *Tmod1*$^{-/-Tg+}$ muscle, Tmod3 and -4 localize to thin filament pointed ends despite weaker binding, demonstrating that strong Tmod–TM binding is not required to correctly target Tmods to the pointed ends.

To further characterize Tmod–TM isoform interactions, we performed a reciprocal experiment to compare directly the relative binding of each Tmod to the different TMs, where blots containing the three aforementioned TMs were overlaid with Tmod1, -3, or -4. The results of this blot overlay show that both Tmod1 and -4 bound somewhat more strongly to α_{slow}-TM than to β-TM but not at all to M9R α_{slow}-TM. In contrast, Tmod3 bound to M9R α_{slow}-TM to the same extent as to wild-type α_{slow}-TM and more poorly to β-TM (Fig. 6, B, C, and E). The ability of Tmod3 but not Tmod1 or -4 to bind to M9R α_{slow}-TM suggests that Tmod3 has divergent sequence requirements for TM binding. Our blot overlay data appear to contradict previous blot overlay and other binding experiments showing that residues 1–130 of chicken Tmod4 bind more strongly to N-terminal α_{fast}-TM peptides than do residues 1–130 of chicken Tmod1 (Greenfield and Fowler, 2002). However, the truncated Tmods may be missing a portion of an additional TM-binding site (Kostyukova et al., 2006), thereby affecting the overall avidity of the Tmod–TM interaction. This confounding variable prevents side by side comparison of the results in these two studies. In conclusion, the results of these blot overlays show that Tmod1 binds most strongly to striated muscle TMs, with Tmod4 binding less well and Tmod3 displaying the weakest interaction. This

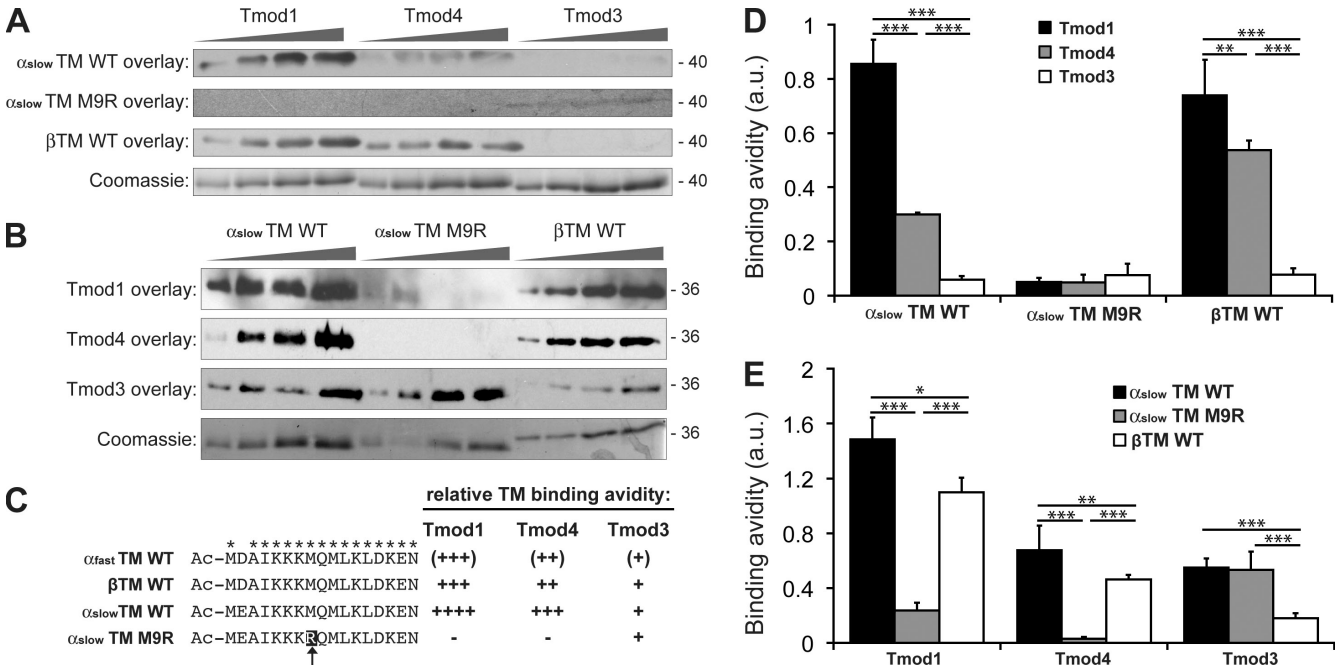

Figure 6. **Tmod3 and -4 bind to striated muscle TMs more weakly than does Tmod1.** (A) Increasing amounts of Tmods were separated by SDS-PAGE, transferred to nitrocellulose, and overlaid with wild-type (WT) α_{slow}-TM (first row), M9R mutant α_{slow}-TM (second row), or β-TM (third row). (B) Increasing amounts of TMs were separated by SDS-PAGE, transferred to nitrocellulose, and overlaid with Tmod1 (first row), -4 (second row), or -3 (third row). Parallel Coomassie-stained gels show loading (fourth row). (A and B) Molecular mass is indicated in kilodaltons. (C) Relative binding strengths among Tmods and TMs were scored semiquantitatively based on visual inspection of blots. Predicted binding between Tmods and α_{fast}-TM (parentheses) is based on sequence identity between the N-terminal regions of α_{fast}-TM and β-TM where Tmods bind (Stone and Smillie, 1978; Helfman et al., 1986). Asterisks indicate conserved residues. The arrow shows the location of the nemaline myopathy–causing M9R mutation. (D and E) Binding avidities were quantified using densitometry by normalizing band intensities from the blots to the corresponding Coomassie-stained bands. x-axis labels refer to the protein that is overlaid, whereas data series refer to the immobilized protein. Note that relative binding avidities can only be compared within each individual blot overlay, demarcated by tick marks, and not from one TM to the next (in D) or from one Tmod isoform to the next (in E) because of variations in antibody binding and blot exposure times. *, $P < 0.05$; **, $P < 0.01$; ***, $P < 0.001$. $n = 4$ lanes/group. Data are mean ± SEM. a.u., arbitrary unit.

indicates that altered Tmod–TM interactions permit correct regulation of thin filament length in skeletal muscle but raises the possibility that substitution of Tmod3 for Tmod1 may affect muscle function.

Deletion of Tmod1 depresses muscle contractility and locomotor behavior

To examine the functional effects of replacing the strong TM-binding combination of Tmod1 and -4 with the weaker TM-binding combination of Tmod3 and -4, we compared isometric contractility in skeletal muscle from *Tmod1*$^{+/+}$ and *Tmod1*$^{-/-Tg+}$ mice. Architectural experiments on fixed muscle tissue showed that the absence of Tmod1 did not affect physiological cross-sectional area (PCSA; Fig. 7 A) or slack sarcomere length (Fig. 7 B), two important structural parameters. However, contractile tests on isolated EDL muscles from *Tmod1*$^{+/+}$ and *Tmod1*$^{-/-Tg+}$ mice revealed that muscles lacking Tmod1 produced ∼20% less isometric force when supramaximally stimulated at 100 Hz (Fig. 7 C). Normalization of isometric force to PCSA to compute isometric stress showed that muscles from *Tmod1*$^{-/-Tg+}$ mice indeed produced significantly less stress (Fig. 7 D), indicating that the muscle function in *Tmod1*$^{-/-Tg+}$ mice is intrinsically compromised despite normal sarcomere structure (Fig. 4).

Because the absence of Tmod1 attenuates stress production in skeletal muscle, we might expect *Tmod1*$^{-/-Tg+}$ mice to have more generalized locomotor deficits. To address this possibility, we subjected *Tmod1*$^{+/+}$ and *Tmod1*$^{-/-Tg+}$ mice to a battery of behavioral assessments. First, voluntary in-cage activity was monitored by counting running wheel rotations and breaks of a laser beam passing through the cage. We found that *Tmod1*$^{-/-Tg+}$ mice exhibited a striking and statistically significant reduction in voluntary activity (Fig. 8, A and B), which can be a symptom of muscle weakness. In contrast, *Tmod1*$^{-/-Tg+}$ mice did not show deficits in the hanging wire test or the grip strength test (Fig. 8, C and D). It is possible that the weakness varies in a muscle-specific manner, and the particular muscles recruited in the hanging wire and the grip strength tests were not sufficiently weakened to produce a statistically significant outcome. The results of the rotarod test were the least conclusive, with *Tmod1*$^{-/-Tg+}$ mice showing a slight but statistically significant trend toward reduced motor coordination at 4 and 6 mo of age but no differences at 1–2 mo or >12 mo (Fig. 8 E). One possibility is that this behavioral phenotype may have not yet manifested in >12-mo-old *Tmod1*$^{-/-Tg+}$ mice, whereas normal deterioration of wild-type muscles because of age may have obscured the effect of genotype in >12-mo-old mice. This could explain why this behavioral phenotype is most robust at the intermediate ages of 4 and 6 mo. However, it is important to note that the locomotor deficits in *Tmod1*$^{-/-Tg+}$ mice, as determined by these behavioral assessments, may be caused by impaired neural function rather than acute muscle weakness. Given that Tmod1 is normally expressed in neurons in the brain

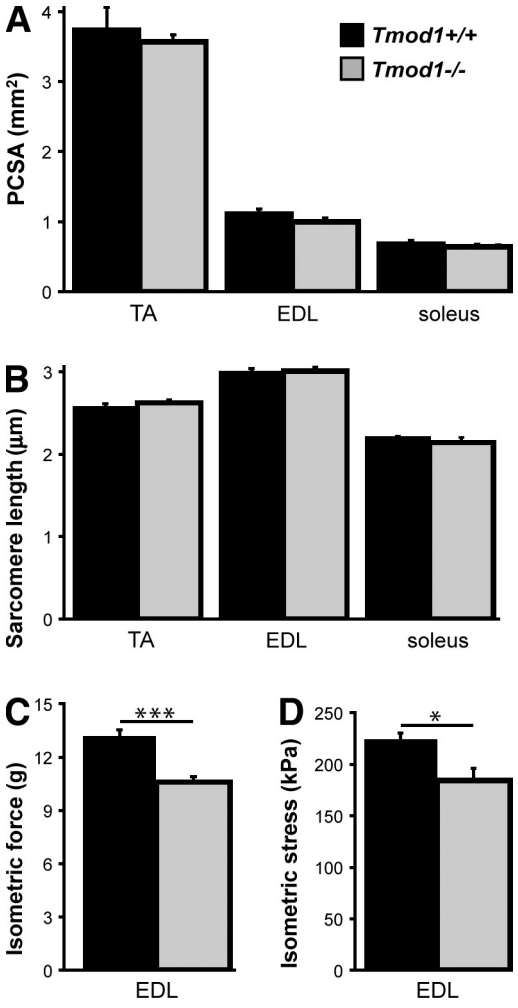

Figure 7. **Deletion of Tmod1 depresses skeletal muscle contractile function.** (A and B) Muscle PCSA (A) and slack sarcomere length (B) are unchanged in $Tmod1^{-/-Tg+}$ mice. (C and D) Isometric force (C) and isometric stress (D) produced by EDL muscle from $Tmod1^{-/-Tg+}$ mice are significantly decreased. *, $P < 0.05$; ***, $P < 0.001$. $n = 8$ muscles/genotype. Data are mean ± SEM.

(Cox and Zoghbi, 2000; Yao et al., 2007) and, therefore, is not present in the neurons of $Tmod1^{-/-Tg+}$ animals (unpublished data), this possibility cannot be excluded.

Deletion of Tmod1 produces fast fiber hypertrophy

It is well established that the level of muscle use directly affects the fiber type composition within a muscle, with heavily recruited muscles trending toward a slower and smaller fiber composition and infrequently recruited muscles trending toward a faster and larger fiber composition (Lieber, 2010). To investigate whether the reduced isometric contractility and impaired locomotor behavior in $Tmod1^{-/-Tg+}$ mice correlated with fiber type changes, we compared the fiber properties of $Tmod1^{+/+}$ and $Tmod1^{-/-Tg+}$ muscles. We found that mean fiber cross-sectional areas in TA and soleus muscles from $Tmod1^{-/-Tg+}$ mice were ~100 µm² larger than normal (Fig. 9, A and B), leading us to believe that a faster fiber phenotype might also be present. Therefore, we used myosin ATPase staining to determine the relative proportions of type 1 (slow) and type 2A/X/B (fast) fibers and whether slow or fast fibers exhibited preferential increases in fiber size. In our strain of mice, wild-type TA and soleus are characterized by 5% and 17% of slow fibers, respectively, which likely reflects the mouse strain mixed background of FVBN/129SVJ/C57Bl6 (McKeown et al., 2008). We found that both TA and soleus muscles from $Tmod1^{-/-Tg+}$ mice exhibited an increased proportion of fast fibers at the expense of a decrease in slow fibers (Fig. 9 C). The muscle-wide increases in fiber cross-sectional area were driven mainly by increases in the size of fast fibers. Namely, the size of slow fibers was unchanged in $Tmod1^{-/-Tg+}$ TA and soleus muscles, but the size of fast fibers was significantly increased (Fig. 9 D). To confirm that fiber type changes correlate with MHC isoform changes, we used SDS-PAGE to separate MHC isoforms and determine MHC isoform composition, and we found that $Tmod1^{-/-Tg+}$ muscles indeed exhibit a shift toward faster MHC isoform composition (Fig. 9 E). Finally, to ensure that weakness in $Tmod1^{-/-Tg+}$ muscles was not simply an artifact of acute muscle damage, we used Hoechst 33258 staining to quantify the frequency of centralized nuclei in $Tmod1^{+/+}$ and $Tmod1^{-/-Tg+}$ muscles. The $Tmod1^{-/-Tg+}$ muscles did not exhibit a statistically significant increase in centralized nuclei (Fig. 9 F), indicating that $Tmod1^{-/-Tg+}$ mice do not have an increased propensity for muscle damage that would lead to cycles of muscle degeneration/regeneration. Together, these data indicate that the $Tmod1^{-/-Tg+}$ mouse is a novel model of decreased muscle use characterized by fast fiber hypertrophy.

Discussion

In this study, we demonstrate that Tmod3 and -4 can replace the thin filament pointed-end capping function of Tmod1 in developmentally distinct ways. First, in embryonic muscle, Tmod4 (but not Tmod3) caps pointed ends in the absence of Tmod1, allowing myofibril assembly and thin filament length regulation. Second, both Tmod1 and -4 normally cap pointed ends and regulate thin filament lengths in adult muscle, but the recruitment of Tmod3 to the pointed ends in the absence of Tmod1 correlates with depressed isometric stress production. Therefore, Tmod1 appears dispensable for establishing and maintaining the correct thin filament lengths and structure of skeletal muscle. However, impaired isometric contractility in the absence of Tmod1 leads to systemic functional deficits in skeletal muscle and reprograms fibers toward a faster phenotype. Thus, Tmod1 regulates skeletal muscle physiology in a thin filament length–independent manner. This is the first study to show that Tmod isoforms can structurally but not functionally compensate for one another in vivo.

Tmod1 is essential for myofibril assembly and development in cardiac but not skeletal muscle

Previous work has shown a key role for Tmod1 in cardiac myofibril assembly and development. Tmod1-null cardiomyocytes in the embryonic mouse heart completely fail to assemble myofibrils and do not beat, resulting in failure of cardiac looping and aborted development (Fritz-Six et al., 2003; McKeown et al., 2008).

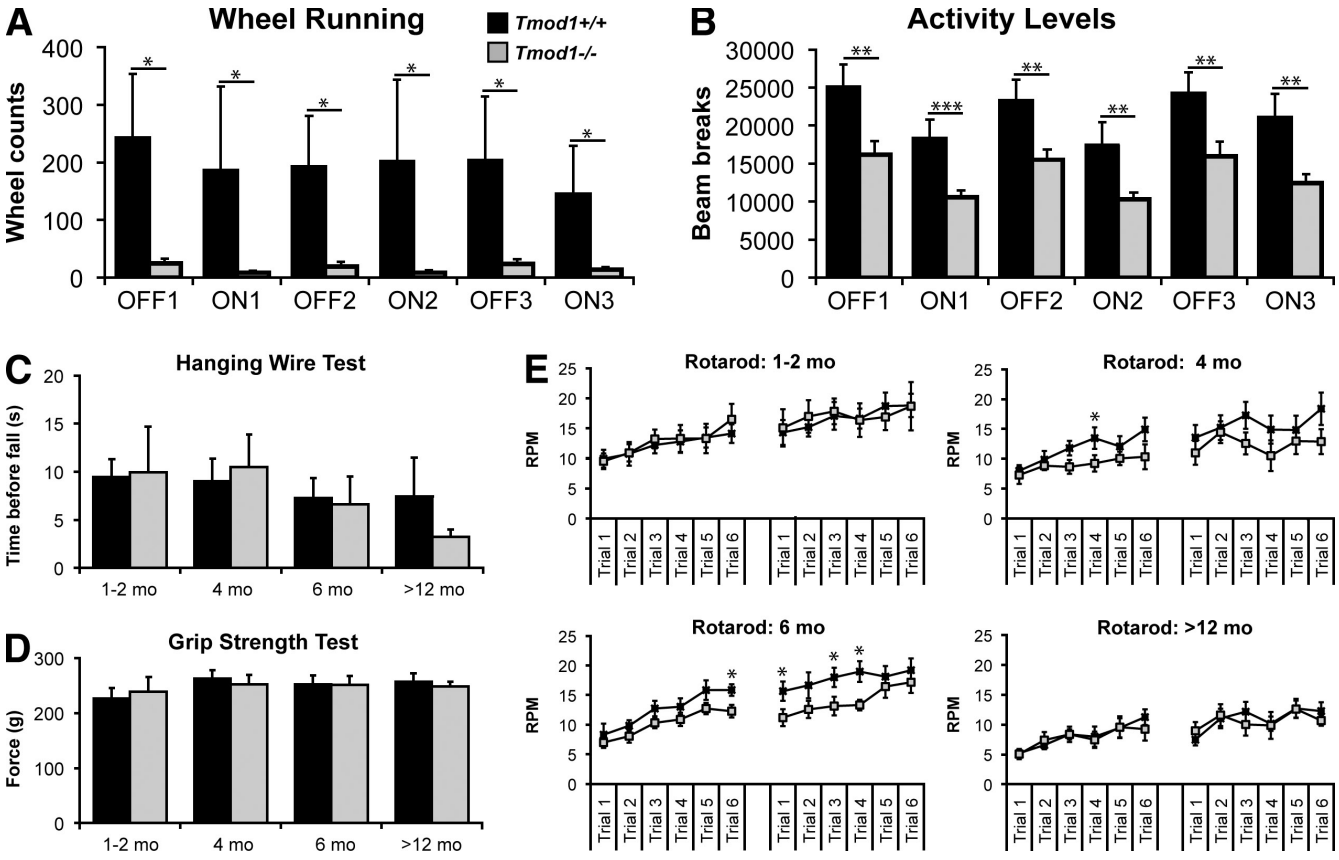

Figure 8. **Deletion of Tmod1 impairs locomotor activity in mice.** (A and B) Voluntary activity in 5–7-mo-old mice was monitored over three consecutive light cycles (12 h off and 12 h on). The number of wheel counts and laser beam breaks was substantially lower in *Tmod1*$^{-/-Tg+}$ animals. (C and D) Muscle strength in mice of various ages was assessed using the hanging wire and grip strength tests. No significant differences in time before falling or grip force were found at any age. (E) Motor coordination was assessed using the rotarod test. No differences in angular speed before falling were found in 1–2-mo-old animals and >12-mo-old animals, but a slight decrease in coordination is evident in 4- and 6-mo-old *Tmod1*$^{-/-Tg+}$ animals. *, $P < 0.05$; **, $P < 0.01$; ***, $P < 0.001$. $n = 6$ (in A and B) or $n = 8$ (in C–E) mice/genotype. Data are mean ± SD.

Instead, actin polymerizes into aberrant aggregates and bundles, suggesting a critical early role for Tmod1 in the in vivo thin filament and myofibril assembly pathway (Chu et al., 2003; Fritz-Six et al., 2003). Further support for a critical role for Tmod1 in cardiac myofibril assembly is that Tmod1-null embryonic stem cells induced to differentiate into cardiomyocytes assemble only a very few myofibrils that are wispy, smaller, and less organized (Ono et al., 2005). Our data argue that, unlike in cardiac myofibrils, Tmod1 is not necessary for the assembly of skeletal myofibrils or for skeletal muscle development. Even in the absence of Tmod1, myoblasts successfully fuse into myotubes, neighboring myotubes align and orient into functioning muscle tissues, and myofibrils assemble completely (Fig. 1 and Fig. S1). Our data also show that Tmod1 is not required for fine-tuning thin filament lengths, both during and after myofibril assembly (Table I). Because Tmod1-null cardiomyocytes fail to assemble myofibrils (Fritz-Six et al., 2003; McKeown et al., 2008) but Tmod1-null skeletal myocytes exhibit no such defect, we can conclude that the mechanisms of myofibril assembly in the heart and in skeletal muscle are different, with Tmod1 playing distinct roles in these different processes. This conclusion is also supported by previous studies in cultured muscle cell models (Gregorio and Fowler, 1995; Almenar-Queralt et al., 1999a; Gregorio and Antin, 2000). Differences in the Tmod isoform inventories and the expression of nebulette versus nebulin in cardiac and skeletal muscle, respectively, may underlie these features of cardiac versus skeletal myofibril assembly (Moncman and Wang, 1995; Millevoi et al., 1998; Almenar-Queralt et al., 1999b; Cox and Zoghbi, 2000; Conley et al., 2001; Ono et al., 2005).

Tmods and TMs regulate thin filament structure at the pointed end

The lack of thin filament length changes in the absence of Tmod1 provides important insights regarding the functions of Tmods at thin filament pointed ends. Tmod1 is a dynamic cap, with Tmod1 moving between its bound ("on") and unbound ("off") states (Littlefield et al., 2001). The proportion of time that Tmods spend capping the thin filament is expected to depend on their avidities for TM-decorated thin filaments. Therefore, we initially considered two possible outcomes of Tmod1 deletion. (1) Thin filaments could lengthen because of a lack of pointed-end capping, allowing new actin subunits to associate with the filament. This outcome would be consistent with the results of Tmod1 antibody inhibition experiments (Gregorio et al., 1995) and perturbations of Tmod1 expression levels in cultured cardiomyocytes (Sussman et al., 1998a; Littlefield et al., 2001) and in *Drosophila melanogaster* (Mardahl-Dumesnil and

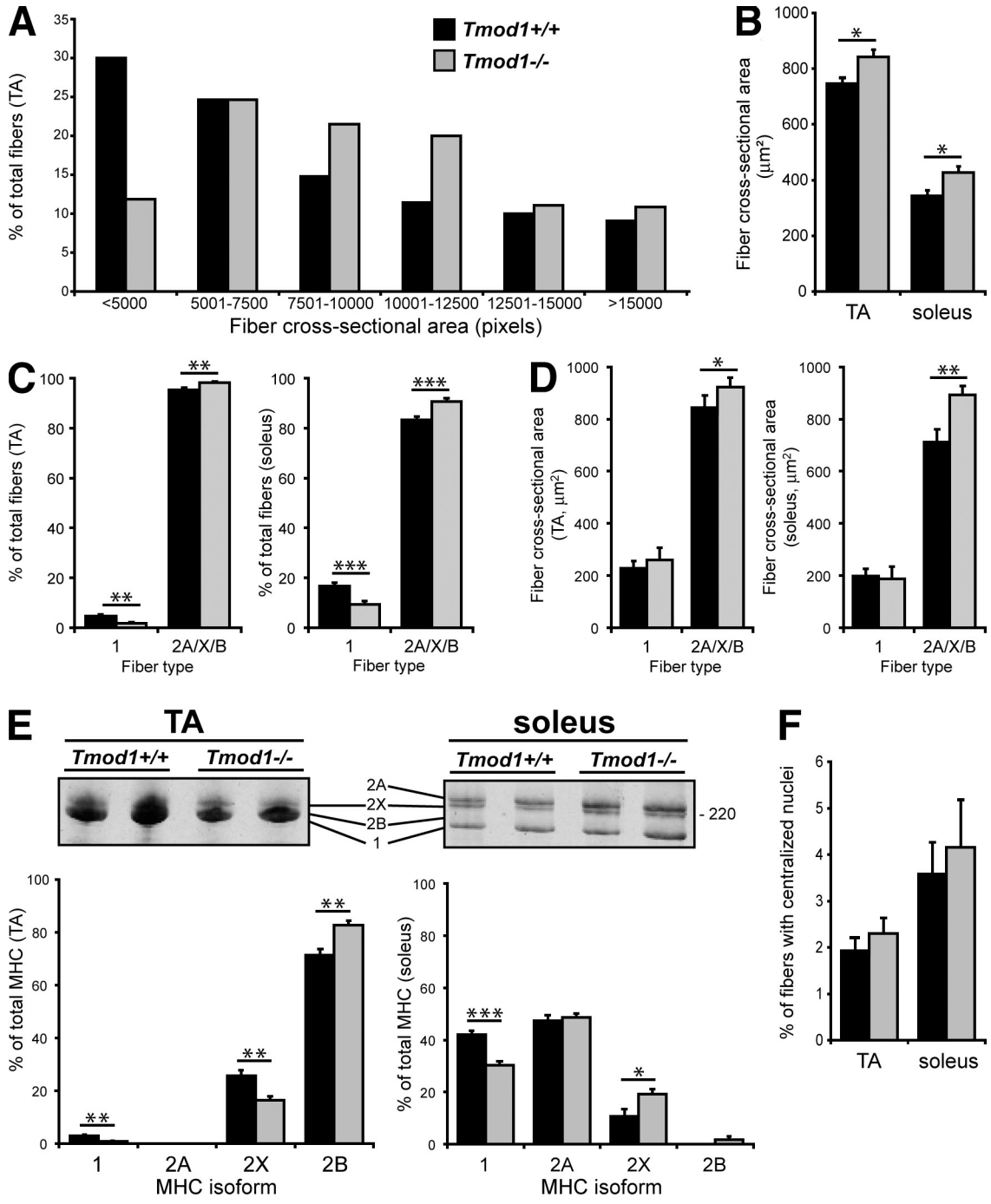

Figure 9. **Deletion of Tmod1 shifts muscle fiber types toward a faster distribution.** (A) The distribution of fiber sizes in the TA was shifted rightward in *Tmod1*$^{-/-Tg+}$ muscle. Graph shows the size distribution of $n = 560$ *Tmod1*$^{+/+}$ fibers and $n = 479$ *Tmod1*$^{-/-Tg+}$ fibers measured from $n = 2$ mice/genotype. (B) The mean fiber cross-sectional area was significantly elevated in both the TA and soleus, suggesting a faster fiber type. (C) The proportion of type 2A/X/B fibers was elevated in the TA and soleus of *Tmod1*$^{-/-Tg+}$ mice at the expense of type 1 fibers. (D) Although there were no significant differences in the size of type 1 fibers, type 2A/X/B fibers were significantly larger in *Tmod1*$^{-/-Tg+}$ TA and soleus. (E) TA and soleus tissue lysates were separated on 8% SDS-PAGE gels. In both TA and soleus, a shift toward faster MHC isoforms was evident in *Tmod1*$^{-/-Tg+}$ mice. Molecular mass is indicated in kilodaltons. (F) No significant differences in centralized nuclei were observed between *Tmod1*$^{+/+}$ and *Tmod1*$^{-/-Tg+}$ muscle. *, $P < 0.05$; **, $P < 0.01$; ***, $P < 0.001$. $n = 4$ (in C and D) or $n = 8$ (in B, E, and F) muscles/genotype. Data are mean ± SEM.

Fowler, 2001; Bai et al., 2007). (2) Alternatively, thin filaments could shorten because of dissociation of TM from the thin filament and resultant thin filament instability and depolymerization (Broschat, 1990; Weber et al., 1994). This has been shown to occur after antibody inhibition of the Tmod–TM interaction in cultured cardiomyocytes (Mudry et al., 2003). Neither of these outcomes occurred in mouse skeletal muscle (Table I). Instead, we uncovered a novel third outcome, that thin filament lengths were unaffected as the result of replacement by other Tmod isoforms, namely Tmod3 and -4, despite the fact that these Tmods bind to striated muscle TMs more weakly than Tmod1 (Fig. 6). Thus, *Tmod1*$^{-/-Tg+}$ skeletal muscle represents a

novel system of reduced thin filament capping without concomitant thin filament length changes. What could account for a reduction in pointed-end capping without concomitant changes in thin filament length? One possibility is that a subset of pointed ends is uncapped in the absence of Tmod1, whereby substoichiometric amounts of other Tmod isoforms maintain thin filament lengths by rapidly shuttling among adjacent thin filaments. Alternatively, *Tmod1*$^{+/+}$ muscle may contain an excess of Tmod3 or -4 that is engaged on pointed ends only when Tmod1 is not present. In *Tmod1*$^{-/-Tg+}$ muscle, thin filaments that are normally capped by Tmod1 may be capped by Tmod3 (in the adult) or by Tmod4 (in both the embryo and the adult) upon Tmod3 or -4 translocation from the sarcoplasm to the pointed ends. In either case, the overall level of pointed-end capping by these different combinations of Tmod isoforms appears to be sufficient to prevent net actin elongation or shortening from the pointed ends in skeletal muscle. We also cannot exclude the possibility that Tmods do not play any role in skeletal muscle thin filament length specification, and as-yet-unknown factors interact with Tmods, TM, nebulin, and actin to determine length, but pursuing such a model is beyond the scope of this work.

Nebulin is not a thin filament ruler

This study extends the previous study that nebulin is not a molecular ruler that dictates thin filament length (Castillo et al., 2009). Instead, thin filaments extend beyond the nebulin N terminus and establish a nebulin-free pointed-end extension whose length ultimately determines the total thin filament length (Castillo et al., 2009; this study). The previous study analyzed an assortment of skeletal muscles from adult rabbits and found that thin filament length varied from 1.13 to 1.31 µm, as determined by Tmod localization (Castillo et al., 2009). In our study, Tmod distances from the Z-line ranged from 1.11 µm in the EDL, to 1.22 µm in the soleus, to 1.26 µm in the embryonic flank, which is consistent with lengths found in rabbit and mouse muscles (Bang et al., 2006; Castillo et al., 2009). We also observed that the nebulin M1M2M3 domain was located at a relatively fixed distance ∼0.84–0.90 µm from the Z-line (Table I), which is closer to the Z-line than Tmod. Thus, we are able to confirm that a nebulin-free pointed-end actin extension determines muscle-specific thin filament lengths (Castillo et al., 2009). Paradoxically, the N terminus of nebulin contains a Tmod1-binding site (McElhinny et al., 2001), even though thin filaments elongate and Tmod1 caps pointed ends ∼200–400 nm away from the nebulin N terminus (Castillo et al., 2009; this study). Therefore, nebulin may only interact with Tmod1 at particular stages of skeletal muscle myofibril assembly or developmental junctures that have not yet been identified. Alternatively, the nebulin N terminus might act at a distance to modulate pointed-end capping by Tmod1 (Fowler et al., 2006).

Tmod1 is a novel regulator of skeletal muscle physiology

Correct specification of thin filament length in skeletal muscle has important functional implications. Thin filament length is one of the principal determinants of the sarcomere length–tension relationship, which quantitatively describes muscle force production at varying degrees of thin and thick filament overlap (Gordon et al., 1966; Granzier et al., 1991). As thin filament length increases or decreases, optimal sarcomere length for muscle force production is expected to increase or decrease, respectively. This property of skeletal muscle has been demonstrated directly in vivo in adult fish, in which fast- and slow-twitch muscles have distinctly different thin filament lengths (Granzier et al., 1991). This property has also been demonstrated in nebulin-null mice, whose skeletal muscle thin filaments are substantially shorter and produce optimal force at a shorter sarcomere length compared with their wild-type counterparts (Gokhin et al., 2009; Ottenheijm et al., 2009). Based on these previous experiments, and the fact that thin filaments from Tmod1-null muscles are of normal length (Table I), we conclude that the optimal sarcomere length range for force production does not differ between *Tmod1*$^{+/+}$ and *Tmod1*$^{-/-Tg+}$ muscles. Despite this, the absence of Tmod1 depresses isometric stress production and locomotor behavior, resulting in alterations in muscle fiber type composition and size consistent with fast fiber hypertrophy (Figs. 7–9). Our myosin ATPase staining measurements show that the increase in fiber size in *Tmod1*$^{-/-Tg+}$ muscles is restricted mainly to fast fibers. Because mouse muscles are overwhelmingly composed of fast fibers even under normal circumstances (Burkholder et al., 1994), changes in fast fibers likely drive the fiber type and size shifts that occur in the absence of Tmod1 (Fig. 9). Thus, our data indicate that the absence of Tmod1 produces fast fiber hypertrophy in a thin filament length–independent manner and, thus, that Tmod1 must regulate skeletal muscle physiology via other mechanisms. However, we cannot exclude the possibility that some aspects of the *Tmod1*$^{-/-Tg+}$ skeletal muscle phenotype may be secondary effects of Tmod1 deletion from neurons and resultant alterations in motoneural input, leading to fiber type switching and/or behavioral effects (Lieber, 2010).

What aspects of muscle contraction aside from thin filament length regulation might be compromised in the absence of Tmod1? One possibility is that Tmod1 modulates actomyosin cross-bridge formation through its interaction with TM at the pointed end. Therefore, in the absence of Tmod1, together with replacement by weaker TM-binding Tmods, TM may not undergo the appropriate conformational changes to permit productive actomyosin cross-bridge cycling. Although this possibility is intriguing, it would require that Tmod1 have a long-range effect along the entire thin filament rather than acting just at the pointed end. It is equally possible that Tmod1 plays a role in coupling mechanical force between myofibrils and the sarcolemma through its association with the extrasarcomeric actin cytoskeleton. Actin filaments are known to associate with costameres, which are multiprotein complexes that establish a link between the sarcolemma and peripheral myofibrils (Craig and Pardo, 1983; Rybakova et al., 2000). Indeed, Tmod1 has been shown to colocalize with β2-spectrin in the costameres of fast muscle fibers in the chicken, suggesting that it may cap actin filaments in the muscle membrane skeleton (Almenar-Queralt et al., 1999b). It is conceivable that misregulation of costameric actin filament length or stability in the absence of Tmod1 leads to mechanical decoupling of peripheral myofibrils from the

sarcolemma and reduces the effective stress produced by the entire muscle. This would be consistent with Tmod1's role in controlling the organization and establishing the mechanical integrity of the membrane-associated spectrin–actin network in other cell types, including lens fiber cells (Nowak et al., 2009) and erythrocytes (unpublished data). Future work will focus on deciphering Tmod1's precise function in regulating the mechanics of skeletal muscle contraction.

Materials and methods

Experimental animals

A viable Tmod1-null mouse line was generated by crossing *Tmod1*$^{lacZ+/-}$ mice (Fritz-Six et al., 2003) with mice that express a Tmod1 transgene under control of the cardiac α-MHC promoter (*Tg(α-MHC–Tmod1)*, denoted as *Tg+* in the text), as previously described in detail (McKeown et al., 2008). Tmod1-null mice with the *Tg(α-MHC–Tmod1)* transgene express Tmod1 exclusively in the heart and in no other tissues and survive into adulthood (McKeown et al., 2008; Nowak et al., 2009). These mice had a mixed FVBN/129SVJ/C57Bl6 background and were maintained as heterozygotes (*Tmod1*$^{+/-Tg+}$). Phenotypic analysis was performed on *Tmod1*$^{+/+}$, *Tmod1*$^{+/+Tg+}$, and *Tmod1*$^{-/-Tg+}$ progeny generated from intercrosses of *Tmod1*$^{+/-Tg+}$ and *Tmod1*$^{+/-}$ mice. In some experiments, intercrosses of *Tmod1*$^{-/-Tg+}$ mice were performed to increase the number of *Tmod1*$^{-/-Tg+}$ progeny. No phenotypic differences were observed between *Tmod1*$^{+/+}$ and *Tmod1*$^{+/+Tg+}$ skeletal muscle, so data from these animals were pooled and referred to in the text as *Tmod1*$^{+/+}$ for simplicity. Genotyping was performed by PCR as described previously (McKeown et al., 2008). All procedures were performed in accordance with animal care guidelines enforced by the Institutional Animal Care and Use Committee at The Scripps Research Institute.

Western blotting

For Tmod1 and -4 Western blots, rabbit antibodies generated against human Tmod1 (R1749) were affinity purified and used at 1 µg/ml (Fowler, 1990), whereas rabbit antisera generated against chicken Tmod4 (R3577; Almenar-Queralt et al., 1999b) were preadsorbed by passing through a human Tmod1 column, and the flow-through was used at a dilution of 1:250. Embryonic and adult muscles were dissected and extracted by homogenization in 4 vol (vol/wet weight) of 9.2 M urea followed by solubilization in 1/5 vol of 5× SDS sample buffer and boiling 5 min. Proteins were separated on 8–16% gradient SDS-PAGE Tris-glycine mini-gels (Invitrogen; Laemmli, 1970). Parallel gels were stained with Coomassie blue or transferred to nitrocellulose for Western blotting (Fowler, 1990). Blots were blocked in 4% BSA in PBS (10 mM $NaHPO_4$, pH 7.4, 150 mM NaCl, and 1 mM EDTA) at room temperature for 2 h and then incubated with primary antibodies diluted in Blitz buffer (4% BSA, 10 mM $NaHPO_4$, pH 7.4, 150 mM NaCl, 1 mM EDTA, and 0.2% Triton X-100) at room temperature for 4 h. After washing in PBS + 0.2% Triton X-100, blots were incubated in HRP-conjugated goat anti–rabbit IgG (1:5,000; Invitrogen) diluted in Blitz for 1 h at 4°C and detection by ECL.

For Tmod3 Western blots, rabbit antibodies generated against human Tmod3 (R5168; Fischer et al., 2003) were preadsorbed by passage of antisera through a human Tmod1 column followed by affinity purification on a mouse Tmod3 column and elution with 4 M $MgCl_2$. Antibodies were dialyzed into PBS followed by dialysis into 50% glycerol in PBS and stored at −20°C. Because of the susceptibility of Tmod3 to proteolysis, embryonic and adult muscles were snap frozen in liquid N_2 and pulverized on dry ice. Tissues were homogenized in 10 vol of 1× SDS sample buffer (vol/wet weight tissue), sonicated, and boiled for 5 min. Embryonic muscle samples were further passed through 16-, 25-, and 30-gauge needles until viscosity was reduced. Aliquots were stored at −80°C and used only once after thawing. Proteins were separated on gradient gels followed by transfer to nitrocellulose as described in the previous paragraph. Blots were blocked by incubation in 4% BSA + 2% donkey serum in PBS overnight at 4°C. Blots were then incubated in primary antibody diluted in 2% donkey serum in Blitz for 2 h at room temperature. After washing, blots were incubated in HRP-conjugated donkey anti–rabbit IgG (1:5,000; Invitrogen) diluted in 2% donkey serum in Blitz for 2 h at 4°C, and bands were detected by ECL.

To control for loading, all blots were stripped and reprobed with monoclonal antibodies against α-tubulin (T9026; 1:3,000; Sigma-Aldrich), stripped, and reprobed again with monoclonal antibodies against actin (C4; 1:10,000; a gift from J.L. Lessard, University of Cincinnati, Cincinnati, OH), both diluted in Blitz, followed by HRP-conjugated anti–mouse secondary antibodies (1:5,000; Invitrogen) and detection by ECL. Each lane in the Western blots is from a muscle obtained from a different individual embryo or adult animal.

Blot overlay

Purified Tmod proteins used were recombinant chicken Tmod1 (Fowler et al., 2003), chicken Tmod4 (Almenar-Queralt et al., 1999b), and human Tmod3 (Fischer et al., 2003). Purified striated muscle TM proteins used were recombinant human α_{slow}-TM, M9R α_{slow}-TM, and β-TM (gifts from S.T. Cooper [University of Sydney, Sydney, New South Wales, Australia] and N.G. Laing [University of Western Australia, Perth, Western Australia, Australia]) expressed in baculovirus and purified as described previously (Akkari et al., 2002). Increasing amounts of purified Tmods or TMs were dissolved in SDS sample buffer and separated by SDS-PAGE on 12 or 15% mini-gels (Laemmli, 1970). Parallel gels were stained with Coomassie blue or transferred to nitrocellulose, and Tmod or TM binding was assessed using a blot overlay (Fowler, 1987). Transferred proteins were bound to the membrane by incubating the nitrocellulose in PBS for 1 h at 65°C, followed by two 5-min washes at 4°C in OverWash buffer (80 mM KCl, 2 mM $MgCl_2$, 1 mM EGTA, 0.2% Triton X-100, and 20 mM Hepes, pH 7.3). The blots were then incubated for 12–18 h at 4°C with 1–2 µg/ml of purified Tmods or TMs in OverWash supplemented with 2% BSA, and excess protein was rinsed with five 5-min washes with OverWash. Bound Tmods or TMs were detected by incubating blots for 12–18 h at 4°C with, as indicated, mouse monoclonal anti-Tmod1 (mAb95; 1 µg/ml; Almenar-Queralt et al., 1999a,b), affinity-purified rabbit anti–chicken Tmod4 (2 µg/ml; Almenar-Queralt et al., 1999b), rabbit antisera to human Tmod3 (R5168; 1:100; Fischer et al., 2003), or rabbit polyclonal antibodies to human erythrocyte TMs (R14; Ursitti and Fowler, 1994). Blots were then rinsed with two consecutive OverWash rinses followed by five 10-min shaking washes. HRP-conjugated mouse or rabbit secondary antibodies were added for 1 h in Blotto (185 mM NaCl, 0.05% Tween 20, 3% powdered skim milk, and 50 mM Tris, pH 7.5). Blots were subsequently washed twice in Blotto and twice in Otto (Blotto minus milk) followed by detection by ECL. Gels and blots were quantified in ImageJ (National Institutes of Health). Note that solid phase blot overlay binding assays are irreversible and do not report affinity (K_d) but rather the avidity of Tmod–TM interactions (Friguet et al., 1985).

Immunofluorescence staining

Timed pregnant mice were sacrificed, and E15.5 embryos were dissected from the uterus in Dulbecco's PBS (D-PBS) for immunofluorescence. Embryos were fixed for 24–48 h at 4°C in 4% PFA in D-PBS, passed through consecutive incubations in 1, 5, and 20% sucrose in D-PBS, embedded in OCT (optimum cutting temperature) medium, cryosectioned, and mounted on microscope slides. Adult TA, diaphragm, EDL, and soleus muscles were dissected from 1-mo-old mice, immersed in ice-cold relaxing buffer (100 mM NaCl, 2 mM KCl, 2 mM $MgCl_2$, 6 mM K_3PO_4, 1 mM EGTA, and 0.1% glucose, pH 7.0), stretched, fixed in 4% PFA, dehydrated in sucrose steps, embedded in OCT medium, snap frozen in liquid N_2, cryosectioned, and mounted on slides. All sections were washed in PBST (D-PBS + 0.1% Triton X-100) and blocked for at least 4 h in 4% BSA + 1% goat serum in PBST. Sections were labeled with primary antibodies diluted in blocking buffer overnight at 4°C, washed in PBST, and then labeled with a fluorescently conjugated secondary antibody mixture in blocking buffer for 2 h at room temperature. The secondary antibody mixture was supplemented with either Alexa Fluor 546–phalloidin or rhodamine-phalloidin (1:200; Sigma-Aldrich) to stain F-actin. Antibodies were as follows: affinity-purified rabbit polyclonal anti–human Tmod1 (R1749; 3–5 µg/ml), rabbit polyclonal antisera to human Tmod3 (R5168bl3c; 1:100) or chicken Tmod4 (R3577bl3c; 1:50), affinity-purified rabbit polyclonal anti–nebulin N-terminal M1M2M3 domain (1357L) and anti–C-terminal M160–164 domain (both at ∼10 µg/ml; gifts from C.C. Gregorio, University of Arizona, Tucson, AZ; McElhinny et al., 2005), mouse monoclonal anti–α-actinin (EA53; 1:200; Sigma-Aldrich) and antimyomesin (B4; 1:1,000; a gift from E. Ehler, Kings College London, London, England, UK), Alexa Fluor 488–conjugated goat anti-rabbit IgG (1:200; Invitrogen), and Alexa Fluor 647–conjugated goat anti–mouse IgG (1:200; Invitrogen). Images of single optical sections were collected at room temperature on a laser-scanning confocal microscope (Radiance 2100; Bio-Rad Laboratories) mounted on a microscope (TE2000-U; Nikon) using 20× NA 0.75 air (Fig. S1) or 100× NA 1.4 oil (Figs. 1–3) objective lenses using LaserSharp 2000 (Bio-Rad Laboratories) or on a confocal microscope (LSM 710; Carl Zeiss, Inc.)

using 100× NA 1.4 oil objective lenses, zoom 1 (Fig. 4 B) or zoom 2 (Fig. 4, C and D; Fig. 5; and Fig. S3), and using ZEN 2008 (Carl Zeiss, Inc.). Images were processed with Photoshop (Adobe), and image figures were constructed in Illustrator (Adobe).

EM

Mice were perfusion fixed in 4% PFA + 1.5% glutaraldehyde in 0.1 M cacodylate buffer on ice followed by dissection of soleus and EDL muscles and incubation for several hours in the same fixative. Fixation was continued overnight in 2.5% glutaraldehyde in 0.1 M cacodylate buffer, and tissues were washed in cacodylate buffer, fixed further in 1% OsO_4 in 0.1 M Na cacodylate buffer for 2 h, again washed in cacodylate buffer, and then dehydrated in graded ethanols followed by propylene oxide and embedded in EMbed 812/Araldite (Electron Microscopy Sciences). Thick sections (1–2 µm) were cut, mounted on glass slides, and stained in toluidine blue for assessment of tissue structure and preservation in the light microscope. Subsequently, 60-nm thin sections were cut, mounted on copper slot grids coated with Parlodion, and stained with uranyl acetate and lead citrate for examination on a transmission electron microscope (Philips CM100; FEI) at 80 kV. Images were collected using a charge-coupled device camera (Megaview III; Olympus).

Distributed deconvolution analysis

Measurements of thin filament lengths in phalloidin-stained myofibrils, as well as the positions of Tmods and N-terminal M1M2M3 epitopes of nebulin relative to the Z-line, were performed using the distributed deconvolution method (Littlefield and Fowler, 2002). This technique uses a plugin developed for ImageJ that generates the best fit of a model intensity distribution function for a given thin filament component (Tmod, F-actin, and nebulin M1M2M3 domain) to an experimental 1D myofibril fluorescence intensity profile (line scan) obtained for each fluorescent probe (anti-Tmod, fluorescent phalloidin, and anti–nebulin M1M2M3). The plugin estimates the spread of light along the line scan and the positions and intensities of each probe with adjustable intensity distributions, using probe-specific models for a repeating series of three to five thin filament arrays along a given myofibril. Image regions containing adequately stretched sarcomeres were identified based on the presence of Tmod or nebulin M1M2M3 doublets or gaps in the phalloidin signal (H-zones). A background-corrected line scan was calculated by averaging the intensity across the width of the myofibril for each point along the selected myofibril length and then subtracting the minimum intensity adjacent to the myofibril from the mean intensity across the myofibril width. Line scans were analyzed by distributed deconvolution using model distributions for phalloidin, Tmod, and nebulin M1M2M3. Thin filament length determined from fluorescent phalloidin line scans was approximately located at the half-maximal intensity on the shoulders of the phalloidin signal with respect to the Z-line. The distances of Tmods and nebulin M1M2M3 from the Z-line were equal to half the distance between the peaks on either side of the thin filament array. Distances in micrometers were calculated by converting pixel sizes to micrometers based on the magnification factor for each image (0.04492 µm/pixel). Tmod lengths were determined using both Tmod1- and Tmod4-immunostained images in *Tmod1*$^{+/+}$ animals but only Tmod4-immunostained images in *Tmod1*$^{-/-Tg+}$ animals. Note that measurements based on phalloidin staining resulted in shorter lengths than measurements based on Tmod staining because of systematic differences in the shapes of the thin filament model profiles that are convolved with Gaussian distributions to estimate the point spread functions of the different fluorescent probes (Littlefield and Fowler, 2002). Differences between genotypes were detected using the Student's *t* test.

Physiological testing

Contractile tests were performed on the fifth toe belly of the EDL, which was selected for its fiber length (L_f) homogeneity and robust tendons (Chleboun et al., 1997). The fifth toe belly of the EDL was excised in ice-cold mammalian Ringer's solution and transferred to a customized muscle-testing apparatus (Sam et al., 2000). The distal tendon was tied down with silk sutures to a rigid post interfaced with dual-mode ergometer (Aurora Scientific). The proximal tendon was secured, also with silk sutures, to a rigid frame attached to a horizontally adjustable platform. Muscle length (L_m) was adjusted such that mechanical slack was eliminated, and laser diffraction verified slack sarcomere length (~3.0 µm). L_m was then measured through a dissecting microscope fitted with an eyepiece crosshair reticule by using a digital micrometer to translate the chamber under the field of view from the proximal EDL origin to the distal myotendinous junction. An electrical stimulator (FHC, Inc.) provided muscle activation via platinum plate electrodes. Muscle twitches were elicited at successively higher stimulation voltages, beginning with 5 V, until maximum twitch force was achieved (typically at ~8 V). Voltage was then doubled to guarantee recruitment of all fibers. Maximum isometric force was elicited by applying a 400-ms train of 0.3-ms pulses delivered at 100 Hz while maintaining constant L_m. A computer algorithm in LabVIEW (National Instruments) was used to trigger the stimulator, acquire signals from the force transducer, and analyze all force–time records. After testing, the muscle was removed from the chamber and weighed. To determine the longitudinal stress within the muscle, force was normalized to PCSA, an anatomical parameter whose value is directly proportional to force-generating capacity (Lieber and Fridén, 2000). L_f was determined for each muscle by multiplying L_m by the characteristic fifth toe EDL L_f:L_m ratio of 0.69 (Chleboun et al., 1997). Muscle mass (M in milligrams), muscle density (ρ = 1.056 g/cm^3), fiber pennation angle (θ = 11.3°), and L_f were used to compute PCSA (in millimeters squared), which is equal to $(M\cos\theta)/(\rho L_f)$. The constants in this formula have been published previously (Mendez and Keys, 1960; Chleboun et al., 1997). Differences between genotypes were detected using the Student's *t* test.

Behavioral testing

Behavioral characteristics were analyzed at the Mouse Animal Models Core at The Scripps Research Institute (http://www.scripps.edu/cnad/inia/animalmodelcores.html). At least six mice per genotype were in all experimental groups. Voluntary in-cage activity of singly housed 5–7-mo-old mice was monitored using an integrated Comprehensive Laboratory Animal Monitoring System (CLAMS; Columbus Instruments). Testing occurred in clear respiratory chambers (20 × 10 × 12.5 cm) equipped with a sipper tube delivering water, food tray connected to a balance, 16 photobeams situated in rows at 0.5-in intervals to detect motor activity, and a running wheel with rotation monitoring. Data were averaged across 12-h intervals corresponding to circadian lights off and lights on epochs. Muscle strength was measured in 1–2-, 4-, 6-, and >12-mo-old mice using the hanging wire and grip strength tests. In the hanging wire test, mice were held so that only their forelimbs contacted an elevated metal bar, and latency to fall was measured up to a maximum of 30 s. The hanging wire test was repeated three times with 30-s rest periods. In the grip strength test, muscle grip force was measured in the forelimbs using a dual-digital grip strength meter with mesh pull bars (Columbus Instruments). Each mouse was first allowed to grip the instrument grid with only its front paws, and then the mouse was gently and steadily pulled back until the grip was released, at which moment the maximal grip strength was recorded by the instrument. This grip strength test was repeated four times with 30-s rest periods. Coordination was measured using the rotarod test with an Roto-Rod Series 8 (IITC Life Sciences). Mice were placed on the stationary rod, which began to accelerate from 10 rpm, and the rpm at fall was recorded. Mice were subjected to six testing bouts per day, which consisted of two sets of three bouts each, with 1 min between each bout and 2 h between each set. The rotarod procedure was repeated across 2 d. Differences between genotypes were detected using the Wilcoxon rank-sum test.

Muscle fiber types and sizes

For determination of fiber type composition, muscles were homogenized in ice-cold homogenization buffer (250 mM sucrose, 100 mM KCl, 5 mM EDTA, and 20 mM Tris, pH 6.8), and protein was then diluted in SDS sample buffer and boiled for 2 min. MHC isoforms were separated on 22-cm-long 8% SDS-PAGE gels and silver stained (Talmadge and Roy, 1993). Densitometry was performed to quantify bands and compute isoform distributions using ImageJ. The sequence of MHC isoforms 1, 2A, 2X, and 2B reflects increasing twitch speed. To measure mean fiber size, transverse muscle cryosections were blocked with 1% BSA followed by a combination of 1.5% normal goat serum and 10% normal rat serum and immunolabeled overnight with polyclonal antilaminin (1:1,000; Sigma-Aldrich) and then for 1 h with Alexa Fluor 594–conjugated goat anti–rabbit IgG (Invitrogen) supplemented with Hoechst 33258 to locate centralized nuclei. Images were collected at room temperature with a digital camera (SPOT RT; Diagnostic Instruments, Inc.) on an epifluorescent microscope (Microphot SA; Nikon) using a 10× NA 0.30 air objective lens. Fiber sizes in laminin-immunostained images were measured using a custom-made applet that thresholded images and computed fiber cross-sectional areas (Gokhin et al., 2008). To determine fiber size distribution, dissected muscles were immersion fixed in 4% PFA and processed for embedding in paraffin by standard procedures. Paraffin sections were cut in the transverse orientation and stained with hematoxylin and eosin (H&E). For myosin ATPase staining (Brooke and Kaiser, 1970), transverse cryosections were preincubated in acidic conditions (pH 4.3), rinsed, and then incubated at 37°C in the presence of ATP and Ca^{2+}, pH 9.75. Sections were then incubated in 2% $CoCl_2$, rinsed, and reacted with 0.5% $(NH_4)_2S$. H&E- and

myosin ATPase–stained sections were imaged using a 20× NA 0.45 air objective lens mounted on a microscope (Axioskop; Carl Zeiss, Inc.) with a charge-coupled device camera (Axiocam; Carl Zeiss, Inc.). In both myosin ATPase– and H&E-stained images, fiber outlines were manually segmented. All images were processed in ImageJ. Differences between genotypes were detected using the Student's *t* test.

Online supplemental material

Fig. S1 shows that Tmod1 is not required for embryonic skeletal myogenesis. Fig. S2 shows that deletion of Tmod1 does not affect levels of major proteins in adult skeletal muscle. Fig. S3 shows that Tmod3 and -4 substitute for Tmod1 in TA, diaphragm, and soleus muscles. Online supplemental material is available at http://www.jcb.org/cgi/content/full/jcb.201001125/DC1.

We thank Malcolm R. Wood for EM, Amanda J. Roberts for behavioral experiments, Jeannette D. Moyer for purification of Tmods, Jawon Lee and Renee Chow for genotyping, and members of the Fowler laboratory for editorial suggestions and helpful discussions.

This work was supported by National Institutes of Health (NIH) grants (HL083464 to V.M. Fowler and AR40050 to R.L. Lieber), a George E. Hewitt Foundation fellowship (to C.R. McKeown), an NIH National Research Service Award postdoctoral fellowship (AR055870 to R.A. Lewis), a National Heart, Lung and Blood Institute Vascular Biology Training grant (HL007195 to D.S. Gokhin), and a National Eye Institute Core Grant for Vision Research (P30-EY12598) for image processing and analysis.

Submitted: 22 January 2010
Accepted: 3 March 2010

References

Akkari, P.A., Y. Song, S. Hitchcock-DeGregori, L. Blechynden, and N. Laing. 2002. Expression and biological activity of Baculovirus generated wild-type human slow alpha tropomyosin and the Met9Arg mutant responsible for a dominant form of nemaline myopathy. *Biochem. Biophys. Res. Commun.* 296:300–304. doi:10.1016/S0006-291X(02)00852-5

Almenar-Queralt, A., C.C. Gregorio, and V.M. Fowler. 1999a. Tropomodulin assembles early in myofibrillogenesis in chick skeletal muscle: evidence that thin filaments rearrange to form striated myofibrils. *J. Cell Sci.* 112:1111–1123.

Almenar-Queralt, A., A. Lee, C.A. Conley, L. Ribas de Pouplana, and V.M. Fowler. 1999b. Identification of a novel tropomodulin isoform, skeletal tropomodulin, that caps actin filament pointed ends in fast skeletal muscle. *J. Biol. Chem.* 274:28466–28475. doi:10.1074/jbc.274.40.28466

Bai, J., J.H. Hartwig, and N. Perrimon. 2007. SALS, a WH2-domain-containing protein, promotes sarcomeric actin filament elongation from pointed ends during *Drosophila* muscle growth. *Dev. Cell*. 13:828–842. doi:10.1016/j.devcel.2007.10.003

Bang, M.L., X. Li, R. Littlefield, S. Bremner, A. Thor, K.U. Knowlton, R.L. Lieber, and J. Chen. 2006. Nebulin-deficient mice exhibit shorter thin filament lengths and reduced contractile function in skeletal muscle. *J. Cell Biol.* 173:905–916. doi:10.1083/jcb.200603119

Brooke, M.H., and K.K. Kaiser. 1970. Muscle fiber types: how many and what kind? *Arch. Neurol.* 23:369–379.

Broschat, K.O. 1990. Tropomyosin prevents depolymerization of actin filaments from the pointed end. *J. Biol. Chem.* 265:21323–21329.

Burkholder, T.J., B. Fingado, S. Baron, and R.L. Lieber. 1994. Relationship between muscle fiber types and sizes and muscle architectural properties in the mouse hindlimb. *J. Morphol.* 221:177–190. doi:10.1002/jmor.1052210207

Castillo, A., R. Nowak, K.P. Littlefield, V.M. Fowler, and R.S. Littlefield. 2009. A nebulin ruler does not dictate thin filament lengths. *Biophys. J.* 96:1856–1865. doi:10.1016/j.bpj.2008.10.053

Chleboun, G.S., T.J. Patel, and R.L. Lieber. 1997. Skeletal muscle architecture and fiber-type distribution with the multiple bellies of the mouse extensor digitorum longus muscle. *Acta Anat. (Basel)*. 159:147–155. doi:10.1159/000147977

Chu, X., J. Chen, M.C. Reedy, C. Vera, K.L. Sung, and L.A. Sung. 2003. E-Tmod capping of actin filaments at the slow-growing end is required to establish mouse embryonic circulation. *Am. J. Physiol. Heart Circ. Physiol.* 284:H1827–H1838.

Clark, K.A., A.S. McElhinny, M.C. Beckerle, and C.C. Gregorio. 2002. Striated muscle cytoarchitecture: an intricate web of form and function. *Annu. Rev. Cell Dev. Biol.* 18:637–706. doi:10.1146/annurev.cellbio.18.012502.105840

Conley, C.A., K.L. Fritz-Six, A. Almenar-Queralt, and V.M. Fowler. 2001. Leiomodins: larger members of the tropomodulin (Tmod) gene family. *Genomics*. 73:127–139. doi:10.1006/geno.2000.6501

Cox, P.R., and H.Y. Zoghbi. 2000. Sequencing, expression analysis, and mapping of three unique human tropomodulin genes and their mouse orthologs. *Genomics*. 63:97–107. doi:10.1006/geno.1999.6061

Craig, S.W., and J.V. Pardo. 1983. Gamma actin, spectrin, and intermediate filament proteins colocalize with vinculin at costameres, myofibril-to-sarcolemma attachment sites. *Cell Motil.* 3:449–462. doi:10.1002/cm.970030513

Fischer, R.S., K.L. Fritz-Six, and V.M. Fowler. 2003. Pointed-end capping by tropomodulin3 negatively regulates endothelial cell motility. *J. Cell Biol.* 161:371–380. doi:10.1083/jcb.200209057

Fowler, V.M. 1987. Identification and purification of a novel Mr 43,000 tropomyosin-binding protein from human erythrocyte membranes. *J. Biol. Chem.* 262:12792–12800.

Fowler, V.M. 1990. Tropomodulin: a cytoskeletal protein that binds to the end of erythrocyte tropomyosin and inhibits tropomyosin binding to actin. *J. Cell Biol.* 111:471–481. doi:10.1083/jcb.111.2.471

Fowler, V.M., N.J. Greenfield, and J. Moyer. 2003. Tropomodulin contains two actin filament pointed end-capping domains. *J. Biol. Chem.* 278:40000–40009. doi:10.1074/jbc.M306895200

Fowler, V.M., C.R. McKeown, and R.S. Fischer. 2006. Nebulin: does it measure up as a ruler? *Curr. Biol.* 16:R18–R20. doi:10.1016/j.cub.2005.12.003

Friguet, B., A.F. Chaffotte, L. Djavadi-Ohaniance, and M.E. Goldberg. 1985. Measurements of the true affinity constant in solution of antigen-antibody complexes by enzyme-linked immunosorbent assay. *J. Immunol. Methods*. 77:305–319. doi:10.1016/0022-1759(85)90044-4

Fritz-Six, K.L., P.R. Cox, R.S. Fischer, B. Xu, C.C. Gregorio, H.Y. Zoghbi, and V.M. Fowler. 2003. Aberrant myofibril assembly in tropomodulin1 null mice leads to aborted heart development and embryonic lethality. *J. Cell Biol.* 163:1033–1044. doi:10.1083/jcb.200308164

Gokhin, D.S., S.R. Ward, S.N. Bremner, and R.L. Lieber. 2008. Quantitative analysis of neonatal skeletal muscle functional improvement in the mouse. *J. Exp. Biol.* 211:837–843. doi:10.1242/jeb.014340

Gokhin, D.S., M.L. Bang, J. Zhang, J. Chen, and R.L. Lieber. 2009. Reduced thin filament length in nebulin-knockout skeletal muscle alters isometric contractile properties. *Am. J. Physiol. Cell Physiol.* 296:C1123–C1132. doi:10.1152/ajpcell.00503.2008

Gordon, A.M., A.F. Huxley, and F.J. Julian. 1966. The variation in isometric tension with sarcomere length in vertebrate muscle fibres. *J. Physiol.* 184:170–192.

Granzier, H.L., H.A. Akster, and H.E. Ter Keurs. 1991. Effect of thin filament length on the force-sarcomere length relation of skeletal muscle. *Am. J. Physiol.* 260:C1060–C1070.

Greenfield, N.J., and V.M. Fowler. 2002. Tropomyosin requires an intact N-terminal coiled coil to interact with tropomodulin. *Biophys. J.* 82:2580–2591. doi:10.1016/S0006-3495(02)75600-2

Gregorio, C.C., and P.B. Antin. 2000. To the heart of myofibril assembly. *Trends Cell Biol.* 10:355–362. doi:10.1016/S0962-8924(00)01793-1

Gregorio, C.C., and V.M. Fowler. 1995. Mechanisms of thin filament assembly in embryonic chick cardiac myocytes: tropomodulin requires tropomyosin for assembly. *J. Cell Biol.* 129:683–695. doi:10.1083/jcb.129.3.683

Gregorio, C.C., A. Weber, M. Bondad, C.R. Pennise, and V.M. Fowler. 1995. Requirement of pointed-end capping by tropomodulin to maintain actin filament length in embryonic chick cardiac myocytes. *Nature*. 377:83–86. doi:10.1038/377083a0

Gunning, P., G. O'Neill, and E. Hardeman. 2008. Tropomyosin-based regulation of the actin cytoskeleton in time and space. *Physiol. Rev.* 88:1–35. doi:10.1152/physrev.00001.2007

Helfman, D.M., S. Cheley, E. Kuismanen, L.A. Finn, and Y. Yamawaki-Kataoka. 1986. Nonmuscle and muscle tropomyosin isoforms are expressed from a single gene by alternative RNA splicing and polyadenylation. *Mol. Cell. Biol.* 6:3582–3595.

Ilkovski, B., N. Mokbel, R.A. Lewis, K. Walker, K.J. Nowak, A. Domazetovska, N.G. Laing, V.M. Fowler, K.N. North, and S.T. Cooper. 2008. Disease severity and thin filament regulation in M9R TPM3 nemaline myopathy. *J. Neuropathol. Exp. Neurol.* 67:867–877. doi:10.1097/NEN.0b013e318183a44f

Kostyukova, A.S., B.A. Rapp, A. Choy, N.J. Greenfield, and S.E. Hitchcock-DeGregori. 2005. Structural requirements of tropomodulin for tropomyosin binding and actin filament capping. *Biochemistry*. 44:4905–4910. doi:10.1021/bi047468p

Kostyukova, A.S., A. Choy, and B.A. Rapp. 2006. Tropomodulin binds two tropomyosins: a novel model for actin filament capping. *Biochemistry*. 45:12068–12075. doi:10.1021/bi060899i

Kostyukova, A.S., S.E. Hitchcock-Degregori, and N.J. Greenfield. 2007. Molecular basis of tropomyosin binding to tropomodulin, an actin-capping protein. *J. Mol. Biol.* 372:608–618. doi:10.1016/j.jmb.2007.05.084

Kruger, M., J. Wright, and K. Wang. 1991. Nebulin as a length regulator of thin filaments of vertebrate skeletal muscles: correlation of thin filament length, nebulin size, and epitope profile. *J. Cell Biol.* 115:97–107. doi:10.1083/jcb.115.1.97

Labeit, S., T. Gibson, A. Lakey, K. Leonard, M. Zeviani, P. Knight, J. Wardale, and J. Trinick. 1991. Evidence that nebulin is a protein-ruler in muscle thin filaments. *FEBS Lett.* 282:313–316. doi:10.1016/0014-5793(91)80503-U

Laemmli, U.K. 1970. Cleavage of structural proteins during the assembly of the head of bacteriophage T4. *Nature*. 227:680–685. doi:10.1038/227680a0

Lieber, R.L. 2010. Skeletal Muscle Structure, Function, and Plasticity: The Physiological Basis of Rehabilitation. Third edition. Lippincott Williams & Wilkins, Baltimore, MD. 336 pp.

Lieber, R.L., and J. Fridén. 2000. Functional and clinical significance of skeletal muscle architecture. *Muscle Nerve*. 23:1647–1666. doi:10.1002/1097-4598(200011)23:11<1647::AID-MUS1>3.0.CO;2-M

Littlefield, R., and V.M. Fowler. 2002. Measurement of thin filament lengths by distributed deconvolution analysis of fluorescence images. *Biophys. J.* 82:2548–2564. doi:10.1016/S0006-3495(02)75598-7

Littlefield, R.S., and V.M. Fowler. 2008. Thin filament length regulation in striated muscle sarcomeres: pointed-end dynamics go beyond a nebulin ruler. *Semin. Cell Dev. Biol.* 19:511–519. doi:10.1016/j.semcdb.2008.08.009

Littlefield, R., A. Almenar-Queralt, and V.M. Fowler. 2001. Actin dynamics at pointed ends regulates thin filament length in striated muscle. *Nat. Cell Biol.* 3:544–551. doi:10.1038/35078517

Mardahl-Dumesnil, M., and V.M. Fowler. 2001. Thin filaments elongate from their pointed ends during myofibril assembly in *Drosophila* indirect flight muscle. *J. Cell Biol.* 155:1043–1053. doi:10.1083/jcb.200108026

McElhinny, A.S., B. Kolmerer, V.M. Fowler, S. Labeit, and C.C. Gregorio. 2001. The N-terminal end of nebulin interacts with tropomodulin at the pointed ends of the thin filaments. *J. Biol. Chem.* 276:583–592. doi:10.1074/jbc.M005693200

McElhinny, A.S., S.T. Kazmierski, S. Labeit, and C.C. Gregorio. 2003. Nebulin: the nebulous, multifunctional giant of striated muscle. *Trends Cardiovasc. Med.* 13:195–201. doi:10.1016/S1050-1738(03)00076-8

McElhinny, A.S., C. Schwach, M. Valichnac, S. Mount-Patrick, and C.C. Gregorio. 2005. Nebulin regulates the assembly and lengths of the thin filaments in striated muscle. *J. Cell Biol.* 170:947–957. doi:10.1083/jcb.200502158

McKeown, C.R., R.B. Nowak, J. Moyer, M.A. Sussman, and V.M. Fowler. 2008. Tropomodulin1 is required in the heart but not the yolk sac for mouse embryonic development. *Circ. Res.* 103:1241–1248. doi:10.1161/CIRCRESAHA.108.178749

Mendez, J., and A. Keys. 1960. Density and composition of mammalian muscle. *Metabolism*. 9:184–188.

Miller, J.B. 1991. Myoblasts, myosins, MyoDs, and the diversification of muscle fibers. *Neuromuscul. Disord.* 1:7–17. doi:10.1016/0960-8966(91)90038-T

Millevoi, S., K. Trombitas, B. Kolmerer, S. Kostin, J. Schaper, K. Pelin, H. Granzier, and S. Labeit. 1998. Characterization of nebulette and nebulin and emerging concepts of their roles for vertebrate Z-discs. *J. Mol. Biol.* 282:111–123. doi:10.1006/jmbi.1998.1999

Moncman, C.L., and K. Wang. 1995. Nebulette: a 107 kD nebulin-like protein in cardiac muscle. *Cell Motil. Cytoskeleton*. 32:205–225. doi:10.1002/cm.970320305

Mudry, R.E., C.N. Perry, M. Richards, V.M. Fowler, and C.C. Gregorio. 2003. The interaction of tropomodulin with tropomyosin stabilizes thin filaments in cardiac myocytes. *J. Cell Biol.* 162:1057–1068. doi:10.1083/jcb.200305031

Nowak, R.B., R.S. Fischer, R.K. Zoltoski, J.R. Kuszak, and V.M. Fowler. 2009. Tropomodulin1 is required for membrane skeleton organization and hexagonal geometry of fiber cells in the mouse lens. *J. Cell Biol.* 186:915–928. doi:10.1083/jcb.200905065

Ono, Y., C. Schwach, P.B. Antin, and C.C. Gregorio. 2005. Disruption in the tropomodulin1 (Tmod1) gene compromises cardiomyocyte development in murine embryonic stem cells by arresting myofibril maturation. *Dev. Biol.* 282:336–348. doi:10.1016/j.ydbio.2005.03.015

Ottenheijm, C.A., C.C. Witt, G.J. Stienen, S. Labeit, A.H. Beggs, and H. Granzier. 2009. Thin filament length dysregulation contributes to muscle weakness in nemaline myopathy patients with nebulin deficiency. *Hum. Mol. Genet.* 18:2359–2369. doi:10.1093/hmg/ddp168

Rindt, H., A. Subramaniam, and J. Robbins. 1995. An in vivo analysis of transcriptional elements in the mouse alpha-myosin heavy chain gene promoter. *Transgenic Res.* 4:397–405. doi:10.1007/BF01973758

Rybakova, I.N., J.R. Patel, and J.M. Ervasti. 2000. The dystrophin complex forms a mechanically strong link between the sarcolemma and costameric actin. *J. Cell Biol.* 150:1209–1214. doi:10.1083/jcb.150.5.1209

Sam, M., S. Shah, J. Fridén, D.J. Milner, Y. Capetanaki, and R.L. Lieber. 2000. Desmin knockout muscles generate lower stress and are less vulnerable to injury compared with wild-type muscles. *Am. J. Physiol. Cell Physiol.* 279:C1116–C1122.

Stone, D., and L.B. Smillie. 1978. The amino acid sequence of rabbit skeletal alpha-tropomyosin. The NH2-terminal half and complete sequence. *J. Biol. Chem.* 253:1137–1148.

Sung, L.A., and J.J. Lin. 1994. Erythrocyte tropomodulin binds to the N-terminus of hTM5, a tropomyosin isoform encoded by the gamma-tropomyosin gene. *Biochem. Biophys. Res. Commun.* 201:627–634. doi:10.1006/bbrc.1994.1747

Sung, L.A., V.M. Fowler, K. Lambert, M.A. Sussman, D. Karr, and S. Chien. 1992. Molecular cloning and characterization of human fetal liver tropomodulin. A tropomyosin-binding protein. *J. Biol. Chem.* 267:2616–2621.

Sussman, M.A., S. Baqué, C.S. Uhm, M.P. Daniels, R.L. Price, D. Simpson, L. Terracio, and L. Kedes. 1998a. Altered expression of tropomodulin in cardiomyocytes disrupts the sarcomeric structure of myofibrils. *Circ. Res.* 82:94–105.

Sussman, M.A., S. Welch, N. Cambon, R. Klevitsky, T.E. Hewett, R. Price, S.A. Witt, and T.R. Kimball. 1998b. Myofibril degeneration caused by tropomodulin overexpression leads to dilated cardiomyopathy in juvenile mice. *J. Clin. Invest.* 101:51–61. doi:10.1172/JCI1167

Talmadge, R.J., and R.R. Roy. 1993. Electrophoretic separation of rat skeletal muscle myosin heavy-chain isoforms. *J. Appl. Physiol.* 75:2337–2340.

Ursitti, J.A., and V.M. Fowler. 1994. Immunolocalization of tropomodulin, tropomyosin and actin in spread human erythrocyte skeletons. *J. Cell Sci.* 107:1633–1639.

Vera, C., A. Sood, K.M. Gao, L.J. Yee, J.J. Lin, and L.A. Sung. 2000. Tropomodulin-binding site mapped to residues 7-14 at the N-terminal heptad repeats of tropomyosin isoform 5. *Arch. Biochem. Biophys.* 378:16–24. doi:10.1006/abbi.2000.1802

Watakabe, A., R. Kobayashi, and D.M. Helfman. 1996. N-tropomodulin: a novel isoform of tropomodulin identified as the major binding protein to brain tropomyosin. *J. Cell Sci.* 109:2299–2310.

Weber, A., C.R. Pennise, G.G. Babcock, and V.M. Fowler. 1994. Tropomodulin caps the pointed ends of actin filaments. *J. Cell Biol.* 127:1627–1635. doi:10.1083/jcb.127.6.1627

Weber, A., C.R. Pennise, and V.M. Fowler. 1999. Tropomodulin increases the critical concentration of barbed end-capped actin filaments by converting ADP.P(i)-actin to ADP-actin at all pointed filament ends. *J. Biol. Chem.* 274:34637–34645. doi:10.1074/jbc.274.49.34637

Witt, C.C., C. Burkart, D. Labeit, M. McNabb, Y. Wu, H. Granzier, and S. Labeit. 2006. Nebulin regulates thin filament length, contractility, and Z-disk structure in vivo. *EMBO J.* 25:3843–3855. doi:10.1038/sj.emboj.7601242

Yao, W., J. Nathanson, I. Lian, F.H. Gage, and L.A. Sung. 2007. Mouse erythrocyte tropomodulin in the brain reported by lacZ knocked-in downstream from the E1 promoter. *Gene Expr. Patterns*. 8:36–46. doi:10.1016/j.modgep.2007.08.002